https://doi.org/10.5194/essd-2026-570
Preprint. Discussion started: 27 July 2026

Open Access Earth System Science Data Discussions

Field-tested emission factors and temporal allocation factors for air pollutants emitted from industrial sources in China

Tingting Wang [a], Shaofei Kong [a, b*], Xujing Qin [a], Yaduan Zhou [a], Yunkai Feng [a], Yingying Yan [a], Jian Wu [a], Wei Liu [c], Feng Ding [c]

[a] *Department of Atmospheric Sciences, Research Centre for Complex Air Pollution of Hubei Province, School of Environmental Studies, China University of Geosciences (Wuhan), Wuhan 430074, China*

[b] *Collaborative Innovation Center on Forecast and Evaluation of Meteorological Disasters, Nanjing University of Information Science & Technology, Nanjing 210044, China*

[c] *Hubei Province Academy of Eco-Environmental Sciences, Wuhan, China*

Correspondence to: Shaofei Kong (kongshaofei@cug.edu.cn)

Abstract

High accuracy and hourly-resolved emission inventories of air pollutants rely on timely updates of emission factors (EFs) and reliable temporal allocation factors, yet both remain poorly constrained for industrial point sources. In this study, we combined a dilution sampling system with online monitoring instruments to obtain 1-hour resolved mass concentrations of PM_{10}, $PM_{2.5}$, PM_1, black carbon (BC), NOx, SO_2, and CO emitted from five industrial sectors (cement, medicine manufacturing, glass production, textile, iron and steel) in China. Product- and fuel-based EFs were updated, as well as sector-specific hourly allocation factors optimized for air quality modeling. Their emission amounts were calculated using the revised product-based EFs and further compared with those for widely adopted Multi-resolution Emission Inventory for China (MEIC). Our measured EFs deviated from previously reported literature values by 1–4 orders of magnitude. BC EFs ranged from 3.2×10^{-6} to 4.7×10^{-2} g kg^{-1}, which sharply contrasts with the default zero value recommended by official technical guidelines for most industrial categories. The measured

https://doi.org/10.5194/essd-2026-570
Preprint. Discussion started: 27 July 2026

Open Access Earth System Science Data Discussions

BC/$PM_{2.5}$ mass ratios were 0.0136 and 0.0104 for cement and iron and steel sectors, respectively, both lower than literature-reported ratios, implying substantial overestimation of industrial BC emissions in existing studies. Compared with the activity-adjusted 2024 MEIC inventory, $PM_{2.5}$ emissions estimated using our field-measured EFs were 29.6 and 255 times lower for cement and iron and steel, respectively, reflecting the deployment of advanced air pollution control technologies and the urgent need to update outdated EFs for industrial sources. Additionally, MEIC allocated emissions across 7,720 iron and steel grid cells, which drastically overrepresents real factory distribution. Our study adopted geolocated Point-Of-Interest data to identify only 216 actual sites, partially explaining the overestimation for industrial emissions by MEIC.

Hourly temporal allocation factors exhibited two distinct pollutant-specific diurnal patterns: with three distinct peaks for PM_{10}, $PM_{2.5}$, and PM_1 within a single day and a single peak for BC, SO_2, NOx, and CO. For $PM_{2.5}$, normalized hourly allocation factors ranged from 0.016 to 0.055 (averaged as 0.0417 ± 0.0074). Conventional uniform temporal allocation assumptions (e.g., fixed 1/24 hourly weight) fail to capture nighttime and short-duration emission spikes, especially for particles. This work provides ground-truthed EFs and hourly allocation profiles for subcategory industrial sources, which can improve the accuracy and reliability of high-temporal-resolution emission inventories, and support the validation of industrial hourly-contribution partitioning from receptor and air quality model simulations.

Keywords: air pollutant, industrial source, emission factor, temporal allocation factor, emission inventory

https://doi.org/10.5194/essd-2026-570
Preprint. Discussion started: 27 July 2026

Open Access Earth System Science Data Discussions

1 Introduction

Industrial air pollutant emissions exhibit prominent hourly diurnal variability (Tang et al., 2023), while this variability is often inadequately represented in mainstream national emission inventories (Bo et al., 2021; Tang et al., 2023). Such intra-day emission fluctuation arises from differences in industrial processes (Bo et al., 2021), dynamic operating conditions (Brooks et al., 2025), variable fuel properties (Zhang et al., 2024), and air pollution control technologies and efficiencies (Liu et al., 2023). Widely used global and regional emission inventories, including the Emission Database for Global Atmospheric Research (EDGAR) (Crippa et al., 2018; Olivier et al., 1994), Multi-resolution Emission Inventory for China (MEIC) (Zheng et al., 2018), the Regional Emission Inventory in Asia (REAS) (Kurokawa et al., 2013; Ohara et al., 2007), predominantly adopt average, median or single fixed emission factors (EFs) alongside simplified literature-derived temporal allocation scheme for all air pollutants across industrial sectors. These generalized approximations contributed substantially to the uncertainty of emission inventories.

The EFs used in bottom-up industrial emission inventories are often derived from published literature, regulatory default values, or limited measurements, with infrequent updates. The inherent variability of these EFs directly propagated into emission estimates and dominates overall inventory uncertainty (Solazzo et al., 2021). For instance, an uncertainty range of −33% to +92% for BC emission estimates stemming from EF variability was reported (Cai et al., 2023; Zhao et al., 2011). Uncertainty ranges also differ drastically across air pollutants and industrial sectors. For PM emissions from the cement and iron and steel sectors, uncertainty ranges of −3.1% to +75% have been reported (Hua et al., 2016; Liu et al., 2018, 2021, 2024; Wang et al., 2019). The reported uncertainty ranges were beyond ±28% for BC (Tang et al., 2020), −3.9% to +75% for NOx (Bo et al., 2021; Guo et al., 2022; Hua et al., 2016; Liu et al., 2018, 2021, 2024; Tang et al., 2025; Wang et al., 2019; Yan et al., 2024), −0.2% to +75% for SO_2 (Bo et al., 2021; Guo et al., 2022; Hua et al., 2016; Liu et al., 2018, 2021, 2024; Tang et al., 2025; Wang et al., 2019; Yan et al., 2024), and −4.9% to +75% for CO (Chen et al., 2023; Hua et al., 2016; Liu et al., 2018, 2021; Tang et al., 2020), respectively. Cross-inventory comparisons covering CO, NOx, SO_2, $PM_{2.5}$, and PM_{10} reveal severe

https://doi.org/10.5194/essd-2026-570
Preprint. Discussion started: 27 July 2026

inconsistencies driven by divergent EFs adopted in peer-reviewed literature and official inventory guidelines (Kong et al., 2024; Saikawa et al., 2017). Literature-based EFs cannot capture the differences in control technology, fuel types, and operational practices across facilities and regions (Liu et al., 2015; Zhao et al., 2008). Recent source-specific field measurements indicated that dynamic and site-measured EFs reduce reliance on static average EFs and empirical assumptions in conventional inventories (Tang et al., 2023). Nevertheless, direct stack measurement campaigns remain scarce for most industrial sectors. To resolve temporal variability, former studies commonly rely on pre-defined temporal allocation profiles to disaggregate annual/monthly total emissions into a finer temporal scale (Crippa et al., 2020; Wu et al., 2024a). However, these profiles are mainly built on aggregate activity statistics, regulatory guidelines, or empirical assumptions rather than direct continuous emission observation (MEE, 2024; U.S. EPA, 2021). Uniform, oversimplified diurnal patterns or even the same allocation profiles are commonly assigned to all industrial plants and air pollutants indiscriminately (Crippa et al., 2020; Pham et al., 2008; Sowden et al., 2008). Such simplifications fail to reflect pollutant-specific emission dynamics across diverse sub-type industrial sources, introducing large uncertainties or even errors into hourly emission estimates (Guevara et al., 2025; Wu et al., 2024a), which further introduce biases in simulating corresponding air pollutant concentrations (Guevara et al., 2025).

Prior studies have utilized Continuous Emission Monitoring System (CEMS) data to develop hourly NOx emission inventories for coal-fired power plants (Gu et al., 2022) and industrial facilities (Sun et al., 2023). However, CEMS dataset suffers notable data-quality limitations. incomplete flue gas flow records often force researchers to substitute theoretical flue gas rates (Tang et al., 2023). Independent validation with satellite observations has also indicated that CEMS-reported SO_2 reductions at coal-fired power plants may not always correspond proportionally to satellite-derived SO_2 changes, highlighting the necessity of independent validation of CEMS data (Karplus et al., 2018). A more critical limitation of China's current CEMS network is its limited monitoring scope, with only NOx and SO_2 routinely monitored. Particles and other gaseous air pollutants are not recorded, although exhibit unique diurnal emission cycles distinct from NOx and SO_2.

https://doi.org/10.5194/essd-2026-570
Preprint. Discussion started: 27 July 2026


Open Access Earth System Science Data Discussions

Without this hourly monitoring, former studies rely on proxy data including operating schedules (Pham et al., 2008), energy consumption (Crippa et al., 2020; Guevara et al., 2021), industrial production (Crippa et al., 2020; Wu et al., 2024a), or electricity demand (Guevara et al., 2021) to allocate hourly emissions. This method neglects inter-pollutant differences in emission formation mechanisms, physicochemical transformation processes and pollution control efficiencies. A fixed uniform hourly allocation factor of 1/24 was even adopted for air pollutants emitted from industrial sources (Pham et al., 2008; Sowden et al., 2008), which are quite different from real situations. The high nighttime emission concentrations of air pollutants from industrial processes are easily smoothed out.

Recent datasets including the EDGAR temporal profiles and CAMS-TEMPO provide sector, country, and pollutant-specific temporal profiles, yet they remain largely based on indirect proxy variables and generalized temporal patterns (Crippa et al., 2020; Guevara et al., 2021). Wu et al. (2024a) emphasized that static daily/hourly allocation parameters introduce extra uncertainties by failing to capture the variation with time or region. Biased temporal allocation profiles directly distort simulated ambient pollutant concentrations and their diurnal cycles (Guevara et al., 2025). Therefore, measurement-based and pollutant-specific temporal profiles are urgently required to characterize real industrial emission fluctuations and improve both high-temporal resolution emission inventories and air quality modeling performance.

To sum up, comprehensive field stack measurements were conducted here for cement, medicine, glass, textile, and iron and steel sectors in China. A dilution sampling system coupled with online analyzers was deployed to obtain hourly stack concentrations of PM_{10}, $PM_{2.5}$, PM_1, BC, NOx, SO_2, and CO. The objectives are to: (1) derive field-measured EFs and compare them against values from official guidelines and published literature; (2) develop concentration-weighted hourly temporal allocation factors for them; and (3) quantify emission discrepancies between our updated inventory and the activity-adjusted MEIC inventory and identify underlying driving factors. This work provides observationally constrained parameters to advance high-temporal-resolution industrial emission inventories and refine corresponding air quality modelling outputs.

https://doi.org/10.5194/essd-2026-570
Preprint. Discussion started: 27 July 2026

2 Materials and methods

2.1 Sampling site and field measurements

In-situ stack sampling campaigns were carried out at facilities including cement, glass, medicine, textile, and iron and steel sectors. Table S1 summarizes the production type and capacity, fuel type, daily operating hours, stack height, sampling locations, and pollution-control devices for flue gas. The medicine and glass facilities adopted natural gas-fired boilers, whereas cement, textile, and iron and steel facilities used coal or coke as raw fuel. All sampled facilities except medicine plant were equipped with dust-removal devices. Detailed descriptions are listed in Supplementary Table S1.

The field sampling setup and dilution sampling system are illustrated in Figure 1. Flue gases were sampled isokinetically via a stainless probe and introduced into a dilution channel for dehumidification and uniform mixing with dry and purified air before instrumental detection (Huang et al., 2021; Kong et al., 2013). The continuous monitoring of particulate matter (PM_{10}, $PM_{2.5}$, and PM_1), black carbon (BC), and gaseous air pollutants (NOx, SO_2, and CO) were measured using a Grimm-180 optical particle analyzer (Yuan et al., 2016), an AE33 aethalometer (Drinovec et al., 2015), and a TH-890C flue gas analyzer (Wuhan Tianhong Ltd., China; Qin et al., 2026), respectively. Supplementary Table S2 provided monitoring duration, temporal resolution, data availability rate.

https://doi.org/10.5194/essd-2026-570
Preprint. Discussion started: 27 July 2026

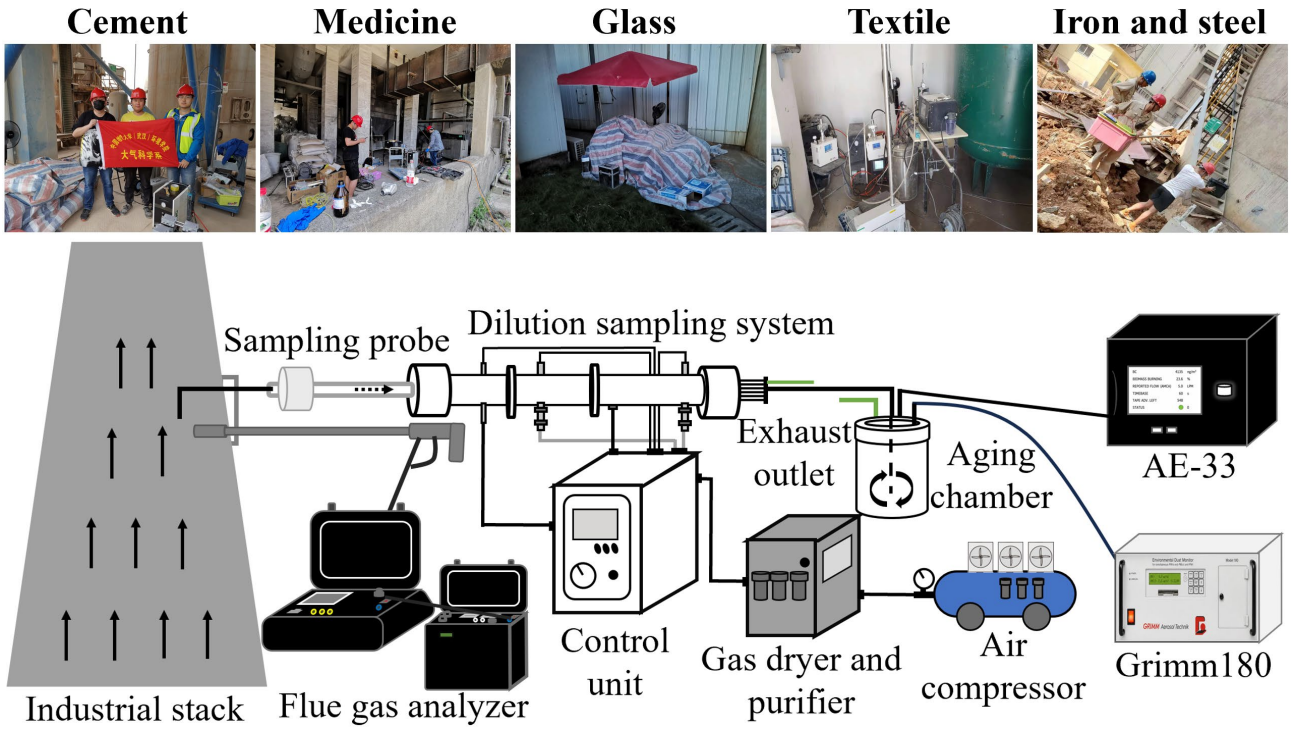

Figure 1. Field sampling setup for stack emission monitoring across the cement, medicine, glass, textile, and iron and steel sectors. The upper panels show field sampling sites, and the lower panel illustrates the connection of the dilution sampling system and online measurement instruments.

2.2 Calculation of concentration-derived temporal allocation factors

Pollutant-specific hourly allocation factors ($f_{i,k,h}$) were calculated by normalizing hourly measured pollutant concentrations against the total 24-hour cumulative concentration, assuming stable flue gas flow throughout each sampling period (Eq. 1):

$$f_{i,k,h} = \frac{C_{i,k,h}}{\sum_{t=1}^{24} C_{i,k,t}} \quad (1)$$

where $C_{i.k,h}$ is the measured mass concentration of pollutant k, from enterprise i during hour h, and t denotes the hour of the day. The concentration-derived hourly allocation factors derived here were compared with previously published temporal profiles (Supplementary Table S3).

https://doi.org/10.5194/essd-2026-570
Preprint. Discussion started: 27 July 2026

Open Access Earth System Science Data Discussions

2.3 Emission factor calculation

EFs for PM_{10}, $PM_{2.5}$, PM_1, BC, NOx, SO_2, and CO were calculated based on measured mass concentrations and production data via Equation (2).

$$EF_{i,k} = \frac{C_{i,k} \times V_i}{A_i} \quad (2)$$

where $EF_{i,k}$ represents the emission factor for pollutant k from enterprise i (unit: g kg^{-1} or g m^{-3}); $C_{i,k}$ is the time-averaged measured mass concentration of pollutant k during sampling (unit: g m^{-3}); V_i is the annual total flue gas volume of enterprise i (unit: m^3); A_i is the corresponding annual activity level, expressed as fuel consumption amount or product output (unit: kg or m^3). All sampling campaigns were conducted under routine stable operating conditions and measured data were considered representative of normal operational periods. Notably, measured SO_2 and CO concentrations at the cement stack fell below instrument detection limits, thus their EFs were referred to literature and international emission inventory guidelines values, as 0.25 and 1 kg t^{-1} clinker, respectively (EEA, 2023; Liu et al., 2024).

2.4 Total emission quantification and comparison with adjusted MEIC inventory

Provincial-level activity data for cement and iron and steel sectors were compiled from official statistical yearbooks and enterprise production records published by the National Bureau of Statistics of China (https://data.stats.gov.cn/, accessed on 15 June 2026). Sectoral total emissions of pollutant k from sector s were calculated as Eq. (3):

$$E_{k,s} = EF_{k,s} \times A_s \quad (3)$$

where $E_{k,s}$ is total emissions of pollutant k from sector s, $EF_{k,s}$ is the emission factor of pollutant k for sector s, and A_s is the corresponding annual activity level, expressed as product output or fuel consumption. Comparative analysis was limited to cement and iron and steel industries due to matching sectoral emission data availability in the MEIC dataset. The latest publicly available MEIC inventory covers 2023 (https://meicmodel.org.cn/, accessed on 15 June

https://doi.org/10.5194/essd-2026-570
Preprint. Discussion started: 27 July 2026

2026). The emissions were rescaled to 2024 levels using provincial activity growth ratios via Eq. (4):

$$E^{adj}_{i,j,p,2024} = E^{MEIC}_{i,j,p,2023} \times \frac{A_{j,p,2024}}{A_{j,p,2023}} \quad (4)$$

where $E^{adj}_{i,j,p,2024}$ is the activity-adjusted 2024 MEIC emission of pollutant i from sector j in province p; $E^{MEIC}_{i,j,p,2023}$ is the raw 2023 MEIC emission; $A_{j,p,2023}$ and $A_{j,p,2024}$ represent the provincial annual activity levels of sector j in 2023 and 2024, respectively, i.e., cement output for cement sector and crude-steel output for iron and steel sector. A uniform activity scaling ratio was applied to all pollutants within each province-sector combination.

Pearson correlation coefficient (r) and normalized mean bias (NMB) were used to evaluate the consistency between our emission estimates and those from the activity-adjusted MEIC inventory. NMB was calculated by Eq. (5):

$$NMB\,(\%) = \frac{\sum_i (E_{this\ study,i} - E_{MEIC,i})}{\sum_i E_{MEIC,i}} \times 100\% \quad (5)$$

Positive NMB values indicate higher emissions in this study relative to adjusted MEIC, and negative values denote lower emissions in our results. Uncertainties in emissions from cement and iron and steel sectors were quantified using Monte Carlo simulations with 20,000 iterations. Provincial activity levels followed normal distributions centered on official 2024 statistics with a 10% coefficient of variation, consistent with standard uncertainty treatment for Chinese industrial bottom-up emission inventories (Solazzo et al., 2021; Zhao et al., 2011). Pollutant- and sector-specific EFs were sampled from distributions parameterized by measured means and standard deviations. Provincial emissions were calculated in each iteration using Eq. (3), summed to national totals, and reported as 95% uncertainty intervals based on the 2.5th and 97.5th percentiles of simulated national emission totals (Li et al., 2023; Zhao et al., 2011).

https://doi.org/10.5194/essd-2026-570
Preprint. Discussion started: 27 July 2026

3 Results and Discussion

3.1 Real-time multi-pollutant stack concentrations

3.1.1 PM_{10}, $PM_{2.5}$ and PM_1

As shown in Figure 2, medicine industry exhibited the highest average PM_{10} concentration of 5.34 ± 0.88 mg m^{-3}, followed by cement (2.61 ± 0.99 mg m^{-3}), textile (1.02 ± 0.45 mg m^{-3}), iron and steel (0.71 ± 0.28 mg m^{-3}), and glass industries (0.19 ± 0.13 mg m^{-3}). Our measured PM_{10} concentrations for cement and iron and steel sectors were markedly lower than previously reported ranges of 3.05–19.38 mg m^{-3} and 25.2–40.8 mg m^{-3}, respectively (Guo et al., 2022; Liu et al., 2019). This sharp reduction can be attributed to tightened emission regulations and broad application of high-efficiency particulate control technologies, including baghouse fabric filters and electrostatic precipitators (Liu et al., 2021; Zhang et al., 2023).

Similar rankings were observed for $PM_{2.5}$, with the highest concentration for medicine industry (5.17 ± 0.84 mg m^{-3}). Cement $PM_{2.5}$ concentration (2.21 ± 0.77 mg m^{-3}) fell below the published range of 2.56–5.04 mg m^{-3} and the single value of 3.55 mg m^{-3} reported by Liu et al. (2019), yet slightly exceeded the 0.09–1.64 mg m^{-3} range documented by Guo et al. (2022). Iron and steel sintering outlet averaged 0.71 ± 0.28 mg m^{-3} $PM_{2.5}$. For medicine, glass, and textile production, the measured values were 5.17 ± 0.84, 0.19 ± 0.13, and 1.02 ± 0.46 mg m^{-3}, respectively. These measurements fill critical gaps in stack-level $PM_{2.5}$ observational dataset for understudied industrial sectors.

PM_1 concentration averaged 1.63 ± 0.44 mg m^{-3} for cement industry, consistent with reported values for clinker production processes (Liu et al., 2019). Iron and steel sintering stack PM_1 concentrations stood at 0.69 ± 0.28 mg m^{-3}. Stack-level PM_1 data remain scarce for medicine, glass, and textile industries. Our field measurements report average PM_1 concentrations of 4.96 ± 0.77, 0.19 ± 0.13, and 0.97 ± 0.47 mg m^{-3} for these three sectors, respectively. This dataset expands available stack-level PM_1 data for neglected industries and improves characterization of industrial particle emissions.

3.1.2 BC

https://doi.org/10.5194/essd-2026-570
Preprint. Discussion started: 27 July 2026

Previous cement industry studies reported elemental carbon (EC) concentrations of 0.02–0.41 mg m^{-3} via thermal-optical analysis (Guo et al., 2022), while our optical BC measurements yielded a much lower mean concentration of 30.5 ± 18.65 μg m^{-3}. Direct numerical comparison between EC and BC is invalid due to fundamentally different analytical principles (Petzold et al., 2013; Pileci et al., 2021). For iron and steel production, previous study indicated EC-based BC fraction of 1.4–2.3% of total PM_{10} mass (Jia et al., 2018). Here, BC concentration was 7.25 ± 3.63 μg m^{-3}, contributing to 1.02 ± 0.65% of PM_{10} mass. Notably, medicine and textile facilities exhibited BC concentrations comparable to or even exceeding heavy industries, demonstrating that light manufacturing sources cannot be overlooked in industrial BC emission inventories and require additional targeted field measurements and refined emission parameterization.

3.1.3 Gaseous pollutant concentrations (NOx, SO_2, and CO)

Measured NOx stack concentrations ranged in 81–227 mg m^{-3}, broadly consistent with CEMS monitoring records for cement and iron and steel industries. Cement kiln tail NOx concentration averaged 81.36 ± 10.91 mg m^{-3}, falling within the reported range of 80–171 mg m^{-3} after DeNOx treatment (Guo et al., 2022). Iron and steel sintering stack NOx concentration reached 227.24 ± 5.42 mg m^{-3}, marginally higher than the reported range of 95–200 mg m^{-3} (Tang et al., 2023). Medicine, glass, and textile boiler NOx concentrations spanned 130–218 mg m^{-3}, comparable to iron and steel, implying that light manufacturing industries represent a substantial and under-recognized source of industrial NOx emissions, and should be improved in emission inventories.

Published CEMS-based iron and steel sector SO_2 concentrations typically range from 30 to 150 mg m^{-3} (Bo et al., 2020; Liu et al., 2022; Tang et al., 2023, 2025; Yi et al., 2021). In contrast, sintering outlet SO_2 measured in this study reached 443.97 ± 11.22 mg m^{-3}, approximately 3–15 times higher than the previously reported range. CEMS concentrations are standardized to fixed reference oxygen levels and averaged over defined time intervals, which smooth short-term concentration spikes. This discrepancy suggests episodic peak SO_2 emissions from industrial point sources are substantially underestimated in CEMS-based assessments, consistent with satellite validation findings (Karplus et al., 2018).

https://doi.org/10.5194/essd-2026-570
Preprint. Discussion started: 27 July 2026

Available stack CO concentration data for industrial sources remain scarce. Cement kiln CEMS CO concentrations previously reported ranged in 12–146 mg m^{-3} (Guo et al., 2022). Our field measured CO concentrations averaged as 20.23 ± 2.35 mg m^{-3} (iron and steel sintering), 10.97 ± 0.99 mg m^{-3} (medicine production), 10.43 ± 2.40 mg m^{-3} (glass production), and 26.39 ± 1.96 mg m^{-3} (textile). All values were generally within or below documented cement kiln ranges, with textile production showing the highest CO concentrations among the measured light manufacturing sectors. The results provide stack CO concentrations for industrial sectors that have been less frequently characterized in previous emission studies.

https://doi.org/10.5194/essd-2026-570
Preprint. Discussion started: 27 July 2026

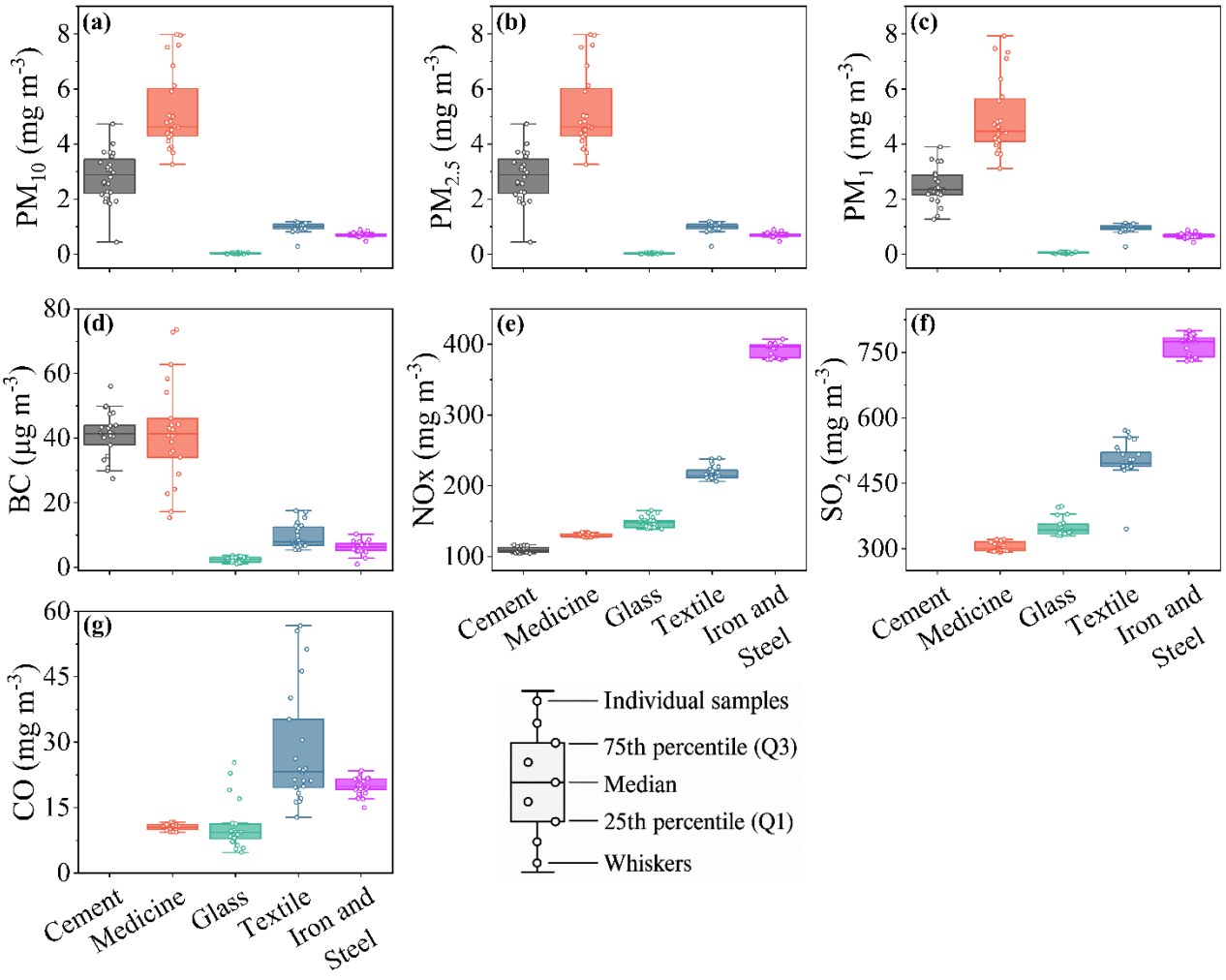

Figure 2. Emission mass concentrations of (a) PM_{10}, (b) $PM_{2.5}$, (c) PM_1, (d) BC, (e) NOx, (f) SO_2 and (g) CO for the cement, medicine, glass, textile, and iron and steel industries. Boxes denote the interquartile range. The horizontal line within each box indicates the median value. Whiskers span the full range of observed data, and circles stand for individual samples. CO and SO_2 were not detected for cement, as their measured signals were below the detection limits.

Overall, our field measurements confirm all major industrial sectors directly emitted $PM_{2.5}$ and BC, in addition to NOx, SO_2, and CO. Although China has achieved substantial reductions in ambient $PM_{2.5}$ concentrations through clean-air actions (Geng et al., 2024; Zhang et al., 2019a),

https://doi.org/10.5194/essd-2026-570
Preprint. Discussion started: 27 July 2026

further improvements toward more stringent air-quality targets require refined quantification of industrial primary fine particles. Previous studies have identified BC and condensable particulate matter as key components of primary emissions from combustion and industrial sources (Cai et al., 2023; Wu et al., 2020). Future industrial emission inventories and pollution control strategies should prioritize improved parameterization of $PM_{2.5}$ including condensable particulate matter and BC.

3.2 Concentration-derived hourly temporal allocation factors

3.2.1 PM_{10}, $PM_{2.5}$ and PM_1

PM_{10} concentrations exhibited a clear trimodal distribution, with prominent peaks during late morning (09:00–12:00) and early evening (18:00–21:00) (Figure 3a). Normalized hourly allocation factors peaked 35% above the daily average at 18:00 and dropped 23% below average at 13:00 (Figure 3h), indicating pronounced short-term emission variability driven by shifting production loads, raw material handling activities, and operating status and efficiency of particulate-control facilities (Tang et al., 2023).

$PM_{2.5}$ showed a sectoral distribution identical to that of PM_{10}, with elevated concentrations for medicine and cement industries (Figure 3b). Its diurnal fluctuation pattern broadly followed that of PM_{10} but with weaker amplitude. The evening peak $PM_{2.5}$ allocation factor rose ~30% above daily mean, while midday values decreased by 15%–20% (Figure 3i). Relative to previously smoother allocation factors (Crippa et al., 2020; Wu et al., 2024b), our field-measured $PM_{2.5}$ allocation factors exhibited far more pronounced short-term fluctuations (Figure 4). This contrast suggests generalized temporal allocation factors dampen actual hourly variability of industrial primary $PM_{2.5}$ emissions.

PM_1 concentrations were consistently lower than PM_{10} and $PM_{2.5}$ yet followed matching sectoral emission rankings (Figure 3c). The diurnal variability of PM_1 was relatively muted, with normalized hourly allocation factors generally varying by approximately 20%–30% around the daily average (Figure 3j). Compared with the former static generalized temporal profiles (Crippa et al., 2020; Guevara et al., 2021), our measured PM_1 allocation factors showed discernible hourly

https://doi.org/10.5194/essd-2026-570
Preprint. Discussion started: 27 July 2026


Open Access Earth System Science Data Discussions

316 fluctuations (Figure 4). This finding suggests that although submicron particle concentrations were
317 less variable than coarser particles, PM_1 allocation factors were not temporally constant. The
318 absence of PM_1-specific diurnal profiles in existing inventories leads to oversimplified
319 representation of industrial submicron particle emissions.

320 **3.2.2 BC**

321 BC showed a distinct sectoral distribution, with the highest concentrations for medicine
322 industry, followed by cement, textile, iron and steel, and glass facilities (Figure 3d). Normalized BC
323 allocation factors peaked at 1.2–1.6 during 10:00–12:00 and declined to 0.75–0.85 during off-peak
324 hours (Figure 3k), indicating that BC concentrations during peak production periods exceeded daily
325 averages by up to 50%–60%. Compared with the smoother temporal allocation factors commonly
326 used in existing inventory datasets (Crippa et al., 2020; Guevara et al., 2021; Wu et al., 2024a),
327 measured BC factors featured far sharper intra-day fluctuations (Figure 4d). As BC is mainly
328 formed during incomplete combustion, transient shifts in combustion conditions, air-fuel mixing
329 ratios, thermal conditions, and process load can produce sharper hourly emission swings than total
330 particulate mass (Bond et al., 2013; Cai et al., 2023). Generic static temporal allocation factors
331 therefore smooth BC emission spikes and fail to capture short-term industrial BC variability.

332 **3.2.3 Gaseous pollutants**

333 NOx concentration-weighted hourly allocation factors remained close to unity throughout the
334 day, deviating within ± (5%–7%) from the daily average with a slight enhancement during the late
335 morning (Figure 3l). Relative to temporal profiles implemented in high-resolution emission
336 inventories (Crippa et al., 2020; Guevara et al., 2021; Wu et al., 2024a), measured NOx curves
337 showed a much flatter diurnal profile (Figure 4). This result underscores the necessity of source-
338 specific NOx temporal allocation factors to accurately represent stable continuous industrial NOx
339 emissions.

340 For SO_2, the concentration-derived hourly allocation factor remained close to the daily mean
341 across most monitoring periods, indicating relatively stable diurnal emission cycles (Figure 3m).
342 Measured SO_2 diurnal profiles were far flatter than previously reported temporal curves for high-
343 temporal-resolution emission inventories (Crippa et al., 2020; Guevara et al., 2021; Wu et al., 2024a)

https://doi.org/10.5194/essd-2026-570
Preprint. Discussion started: 27 July 2026


Open Access Earth System Science Data Discussions

(Figure 4f), demonstrating that universal profiles cannot fully capture source-specific SO_2 variability, especially for continuously operated industrial processes such as iron and steel sintering.

In stark contrast to NOx and SO_2, CO showed strong intra-day variability in its normalized hourly allocation factor (Figure 3n), with pronounced late-morning emission enhancement particularly evident at textile and glass industries. CO formation is highly sensitive to transient incomplete combustion conditions, explaining its amplified hourly fluctuations. When compared with generalized inventory allocation profiles (Crippa et al., 2020; Guevara et al., 2021; Wu et al., 2024a), our measured CO allocation factors displayed much sharper short-term peaks. As CO is a direct tracer of incomplete combustion (Schiferl et al., 2024), generalized allocation factors substantially smooth short-term industrial CO emission peaks.

Overall, generalized universal hourly allocation factors cannot fully represent pollutant-specific industrial emission diurnal cycles. Relative to widely adopted allocation factors from EDGAR, CAMS-TEMPO, Chinese national technical guidelines, and US EPA profiles (Table S3) (Crippa et al., 2020; Guevara et al., 2021; MEE, 2024; Pham et al., 2008; Sowden et al., 2008; U.S. EPA, 2021), our concentration-derived allocation factors exhibit far stronger pollutant- and sector-dependent diurnal variability. These discrepancies carry critical modelling implications for highly variable pollutants including $PM_{2.5}$ and BC, as inaccurate temporal allocation distorts both the timing and magnitude of simulated ambient concentration peaks (Du et al., 2020; Govardhan et al., 2019). Sector-specific and pollutant-derived hourly allocation factors are therefore required to faithfully represent industrial emission dynamics in high-temporal-resolution inventories and air quality models.

https://doi.org/10.5194/essd-2026-570
Preprint. Discussion started: 27 July 2026

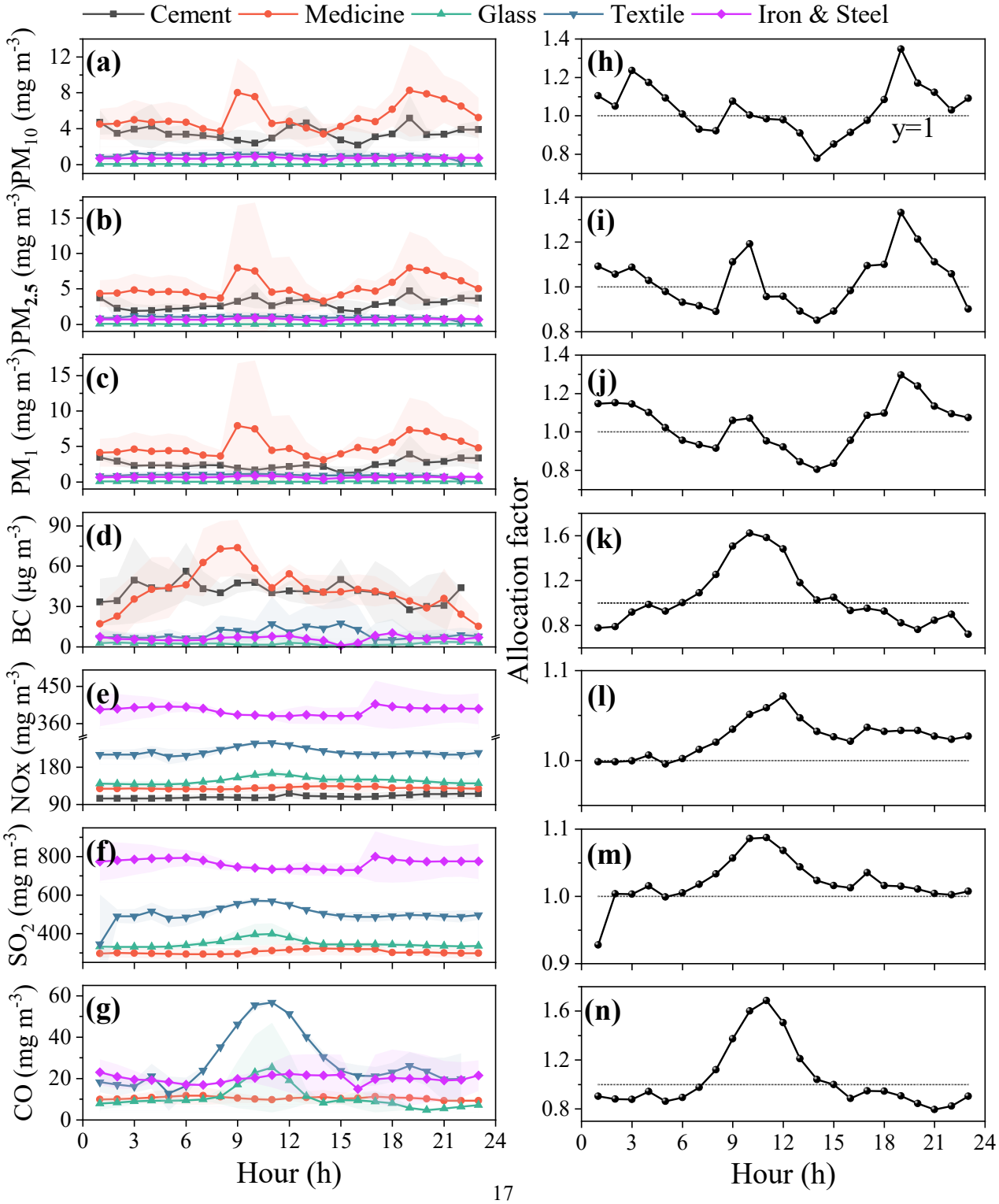

https://doi.org/10.5194/essd-2026-570
Preprint. Discussion started: 27 July 2026

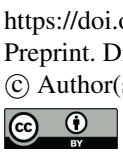

Open Access Earth System Science Data Discussions

Figure 3. Temporal variations in air pollutant concentrations and normalized temporal allocation factors derived for the five industrial emission sources. Panels (a–g) display hourly average concentrations of PM_{10}, $PM_{2.5}$, PM_1, BC, NOx, SO_2, and CO in sequence. Shaded regions represent the standard deviation of hourly pollutant concentrations. Panels (h–n) display the corresponding normalized temporal allocation factors, with the horizontal dashed lines indicating the reference line at unity (normalized factor=1).

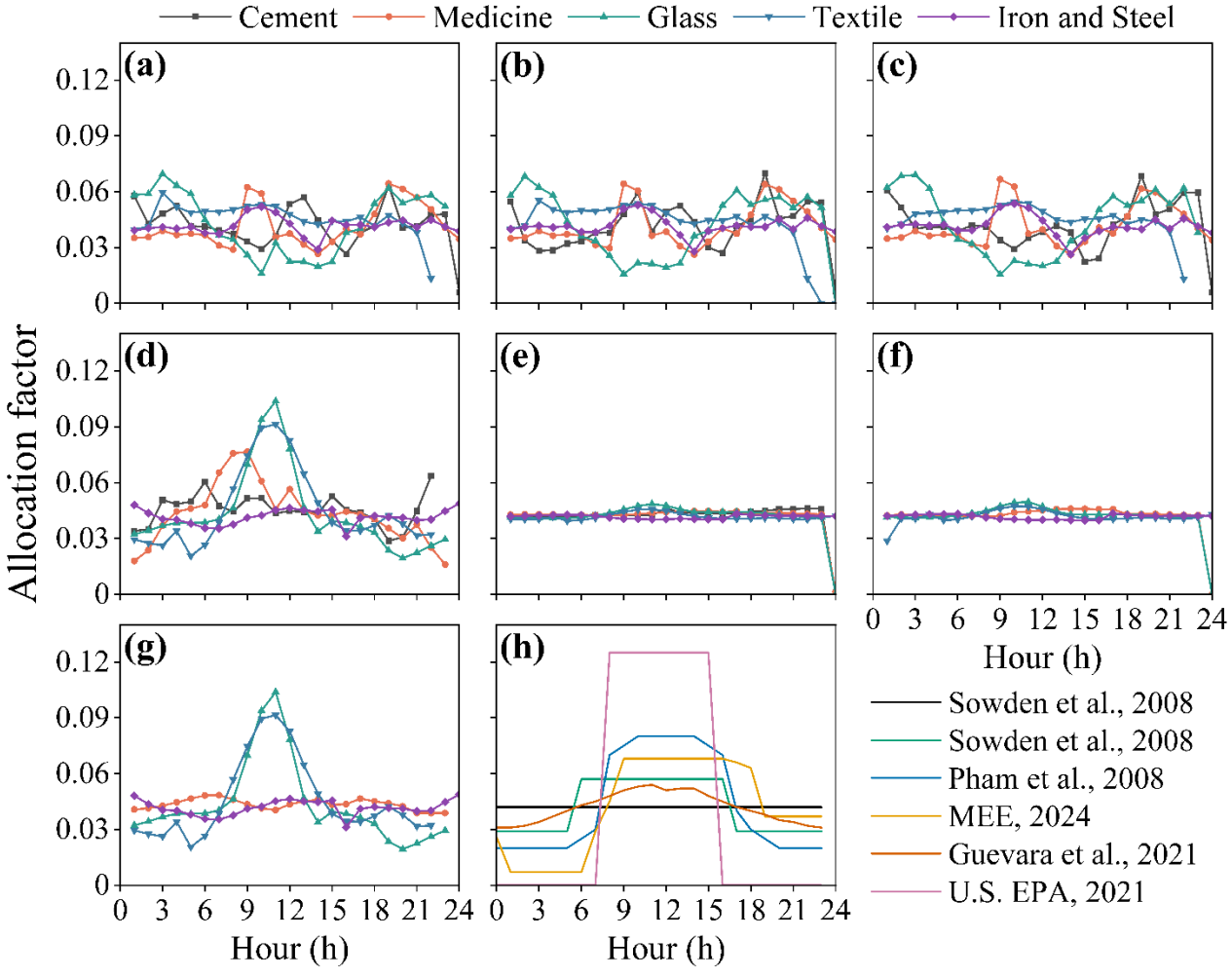

https://doi.org/10.5194/essd-2026-570
Preprint. Discussion started: 27 July 2026

Figure 4. Hourly allocation factors for (a) PM_{10}, (b) $PM_{2.5}$, (c) PM_1, (d) BC, (e) NOx, (f) SO_2, and (g) CO across the five industrial sectors in this study. Panel (h) presents reference hourly temporal allocation factors commonly used in emission models and high-time-resolution emission inventories, including those from Sowden et al. (2008), Pham et al. (2008), MEE (2024), Guevara et al. (2021), and U.S. EPA (2021). Detailed hourly allocation factors shown in this figure are provided in Table S3 in the Supplement file.

3.3 Updated field-measured EFs and comparison with published literature

EFs for PM_{10}, $PM_{2.5}$, PM_1, BC, NOx, SO_2, and CO across five industrial sectors obtained here were compared against literature and official technical guideline values (Figure 5, Tables S12–S19). Measured EFs ranged in 4.5×10^{-4}–6.03 g kg^{-1} product for PM, 3.2×10^{-6}–4.7×10^{-2} g kg^{-1} product for BC, 0.32–146.88 g kg^{-1} product for NOx, 0.25–343.43 g kg^{-1} product for SO_2, and 0.024–12.39 g kg^{-1} product for CO. The wide EF ranges highlight extreme pollutant and sector heterogeneity in industrial emission strengths.

For PM fractions (PM_{10}, $PM_{2.5}$ and PM_1), measured EFs spanned over four orders of magnitude. Relative to literature and guideline benchmarks (Table S13–S15), cement PM_{10} and $PM_{2.5}$ EFs fell near the lower bound of published ranges, while cement PM_1 EFs remained within limited literature range. PM EFs for iron and steel clustered near or below the minimum values of corresponding literature distributions. Medicine sector showed the highest PM EFs (5.60–6.03 g kg^{-1} product), exceeding most official guideline EFs. Glass sector recorded the lowest PM EFs (4.5×10^{-4} g kg^{-1} product), three to four orders of magnitude lower than literature and guideline values (MEE, 2024). These stark sectoral differences in particulate EFs align with previous evidence that industrial PM emissions depend primarily on production processes and end-of-pipe control efficiency (Liu et al., 2021).

BC EFs ranged from 3.2×10^{-6} to 4.7×10^{-2} g kg^{-1} product (Figure 5). For sectors with comparable literature data, particularly glass, cement, and iron and steel, our measured BC EFs were 2–4 orders of magnitude lower than corresponding literature-derived and guideline default EFs

https://doi.org/10.5194/essd-2026-570
Preprint. Discussion started: 27 July 2026

(Guevara et al., 2021; MEE, 2024; Tang et al., 2023). The medicine industry exhibited the maximum BC EF (4.7×10^{-2} g kg^{-1} product), while glass sector yielded the minimum value (3.2×10^{-6} g kg^{-1} product). BC EFs for cement, textile, and iron and steel fell between 10^{-5} and 10^{-4} g kg^{-1} product. These low values are likely associated with complete fuel combustion and effective end-of-pipe particulate control systems (Klimont et al., 2017).

Gaseous pollutant EFs (NOx, SO_2 and CO) also displayed substantial sectoral divergence (Figure 5, Tables S17–S19). Medicine industry recorded the highest NOx and SO_2 EFs across all five sectors (146.88 g kg^{-1} and 343.43 g kg^{-1} product, respectively), implying medicine production as a poorly constrained yet significant gaseous pollutant source driven by complex chemical processes in medicine production (Hu et al., 2019). Glass sector exhibited relatively low NOx and SO_2, and CO EFs, attributable to low-emission furnace technology and upgraded flue gas treatment systems. Remaining sectors generally exhibited intermediate EFs overlapping with published literature ranges, driven by variable fuel compositions, production processes, and emission control levels (Liu et al., 2021). Combined with low PM and BC EFs, these results demonstrate the critical value of updated measurement-based EFs to represent contemporary industrial emission conditions (Solazzo et al., 2021).

Collectively, these findings highlight the urgent need for measurement-refined EFs in industrial emission inventories, particularly for BC. Current Chinese inventory guidelines assign default zero BC EFs to most industrial categories (MEE, 2024), yet non-zero BC emissions were detected for all investigated sectors in this study. This practice leads to full omission or severe underestimation of industrial BC emissions, consistent with updated emission inventory frameworks that explicitly incorporate industrial BC sources (Li et al., 2023; McDuffie et al., 2020).

https://doi.org/10.5194/essd-2026-570
Preprint. Discussion started: 27 July 2026

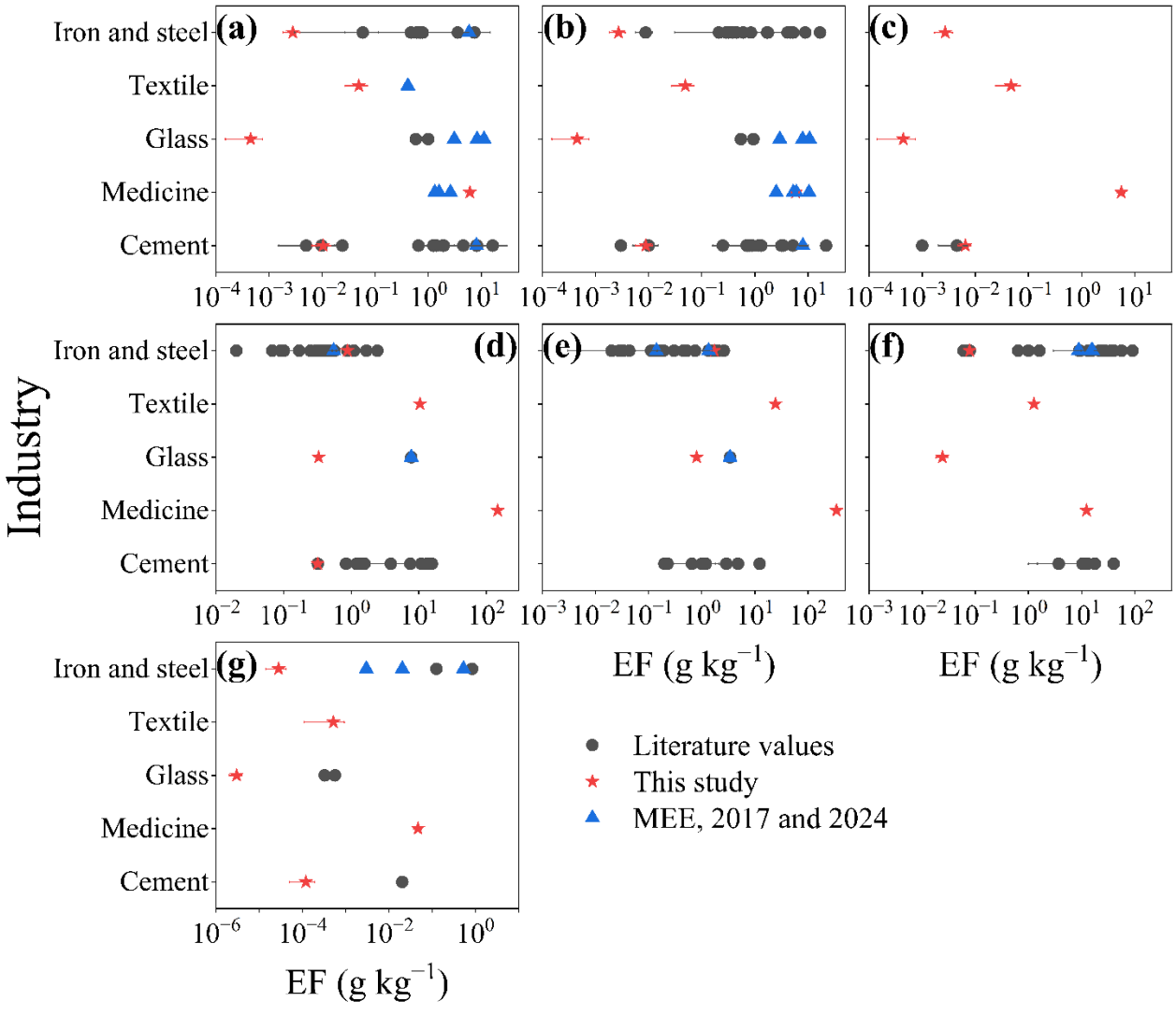

Figure 5. Emission factors (EFs) for (a) PM_{10}, (b) $PM_{2.5}$, (c) PM_1, (d) NOx, (e) SO_2, (f) CO, and (g) BC across major industrial sectors. Grey circles represent literature-reported values, blue triangles denote values from the Ministry of Ecology and Environment of China (MEE), and red stars indicate values derived this study, with horizontal error bars representing uncertainty ranges. Detailed data are provided in Tables S13–S19 in the Supplement file. All EFs displayed here are expressed in g kg^{-1} product.

https://doi.org/10.5194/essd-2026-570
Preprint. Discussion started: 27 July 2026

3.4 Impacts of updated EFs and comparison with the activity-adjusted MEIC inventory

3.4.1 Cement industry

Correlation between our results and activity-adjusted MEIC inventory was strongly pollutant-dependent at provincial scale. High correlation coefficients were found as 0.95 for both PM_{10} and $PM_{2.5}$, 0.92 for NOx, and 0.87 for SO_2, indicating that the two inventories captured consistent provincial emission identities. The slightly weaker SO_2 correlation originates from differences in sulfur-content assumptions, fuel and raw-material properties, desulfurization efficiencies, or provincial allocation schemes (EEA, 2023; Liu et al., 2021).

Substantial negative bias (NMBs = −97%) was observed for both cement PM_{10} and $PM_{2.5}$, while NOx exhibited moderate negative bias (NMB = −17%), and SO_2 displayed positive bias (NMB = +56%). The large negative PM bias arises from three core differences: EF definitions, covered source categories, and temporal representativeness of EFs. MEIC separates cement PM emissions into three independent fractions including clinker production, cement grinding, and fugitive emissions (Liu et al., 2021), with unabated EFs further adjusted by static particulate removal efficiencies (Hua et al., 2016; Lei et al., 2011). In contrast, our EFs were derived from direct measurements at controlled stack outlets, exclusively representing post-treatment organized stack emissions under modern ultra-low emission standards. Ongoing ultra-low-emission retrofits in China's cement industry, together with tightened stack PM limits for cement kilns and kiln-tail waste-heat systems further reduce contemporary stack PM EFs relative to historical or inventory-average assumptions embedded in MEIC. Our lower PM emission estimates therefore reflect both narrower controlled-source coverage (only organized stack outlets) and updated measurement-based EFs representing current low-emission conditions.

Gaseous pollutants (NOx and SO_2) exhibited contrasting bias directions. Moderate negative bias for NOx (NMB = −17%) indicates that measured post-control kiln-tail NOx emissions were broadly comparable to, but slightly lower than, the technology-based assumptions used in MEIC. Cement NOx estimates are affected by kiln type, combustion conditions, low-NOx combustion, and DeNOx removal efficiencies (Liu et al., 2021). Therefore, residual NOx discrepancies reflect

https://doi.org/10.5194/essd-2026-570
Preprint. Discussion started: 27 July 2026

mismatches between measured operating conditions and MEIC's average assumptions for kiln configuration and NOx-control performance. In contrast, SO_2 displayed positive bias (NMB = +56%), indicating higher SO_2 emissions in this study than activity-adjusted MEIC. Cement SO_2 emissions are strongly affected by fuel sulfur content, raw-material sulfur fractions, sulfur retention in clinker or ash, and alkaline absorption inside kiln systems (Lei et al., 2011; Liu et al., 2021; Zhang et al., 2019b). The positive SO_2 bias likely originates from higher effective sulfur release or lower sulfur retention at our measured facilities relative to default assumptions in MEIC.

3.4.2 Iron and steel industry

Provincial correlation coefficients between our inventory and activity-adjusted MEIC inventory ranged from 0.94 to 0.98, with values of 0.98 for both PM_{10} and $PM_{2.5}$, 0.97 for NOx, and 0.94 for SO_2. Our PM emission estimates were 2–3 orders of magnitude lower than MEIC outputs, driven primarily by post-control stack EFs under mandatory ultra-low emission standards, rather than outdated sector-average EFs embedded in MEIC. China's iron and steel ultra-low-emission regulations impose strict limits on organized stack emissions, fugitive dust, and raw material transport losses (MEE, 2019). Previous facility-level analyses confirm strengthened national standards have substantially reduced stack PM emissions for China's iron and steel plants (Bo et al., 2021). Therefore, our lower estimation of PM is dominated by updated measurement-based EFs and dust-control upgrades rather than activity-level differences alone.

Gaseous pollutant bias patterns differed sharply from particulates. Minor negative NOx bias (NMB = −16%) suggests measured NOx emissions were close to MEIC's average technology assumptions, consistent with previous research showing NOx reduction in iron and steel sector were less pronounced than PM and SO_2 reductions during earlier control stages (Bo et al., 2021). In contrast, SO_2 exhibited positive bias (NMB = +127%), indicating our stack SO_2 emissions far exceed activity-adjusted MEIC values. This gap could be related to sintering-dominated SO_2 formation, variable sulfur contents in iron ore, coke breeze, and other raw materials, and assumed desulfurization efficiency, because sintering is a major SO_2-emitting process within integrated steel plants (Wu et al., 2024b). Overall, PM discrepancies mainly reflect updated post-control EF

https://doi.org/10.5194/essd-2026-570
Preprint. Discussion started: 27 July 2026

measurements, whereas SO_2 discrepancies are highly sensitive to sulfur-related process assumptions and desulfurization performance.

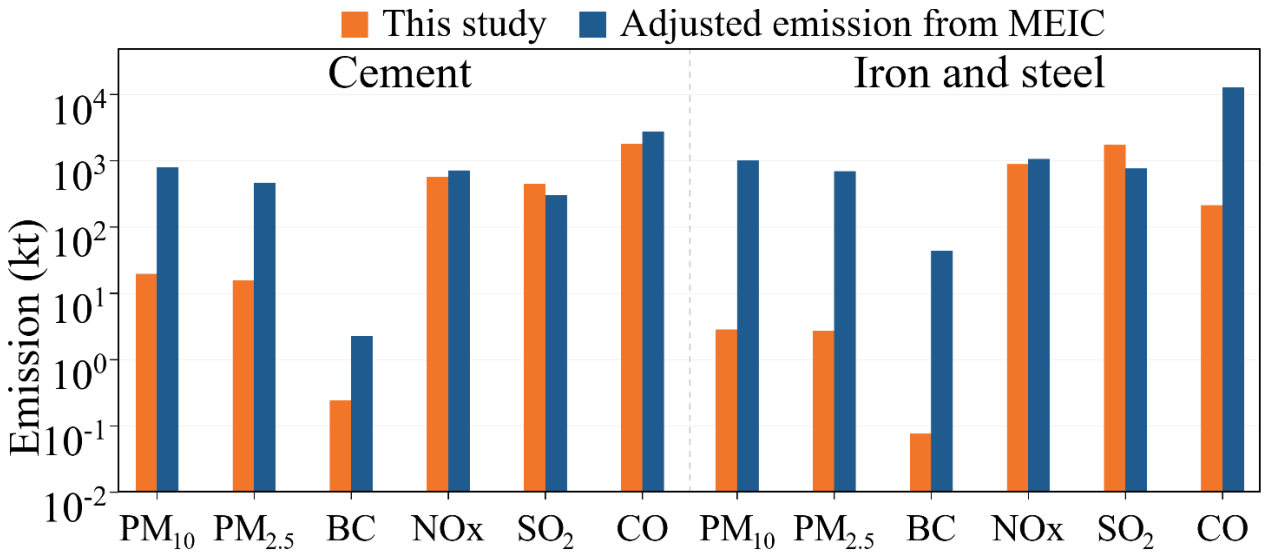

Figure 6. Comparison of air pollutant emission from the cement and iron and steel sectors in 2024. Emissions estimated using the updated EFs obtained in this study are compared with those derived from the activity-adjusted MEIC inventory.

https://doi.org/10.5194/essd-2026-570
Preprint. Discussion started: 27 July 2026

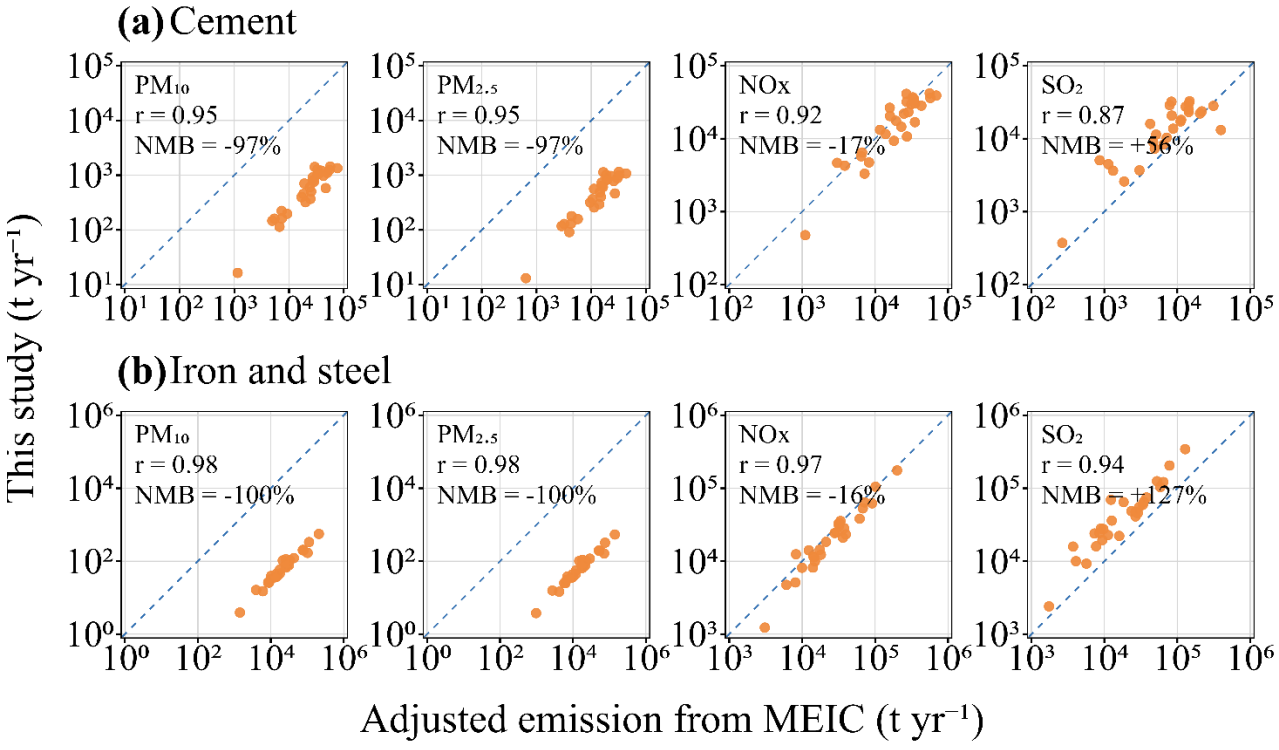

Figure 7. Provincial-level comparison of air pollutant emission amounts (t yr^{-1}) between this study and the activity-adjusted MEIC inventory for 2024. The x-axis represents emissions from the activity-adjusted MEIC inventory, and the y-axis represents emissions estimated in this study. The dashed blue line indicates the 1:1 line. The correlation coefficient (r) denotes the Pearson correlation coefficient between the two inventories, and NMB denotes the normalized mean bias relative to the activity-adjusted MEIC inventory.

Uncertainty analysis (Table S20) revealed that PM emissions generally carry wider uncertainty ranges than gaseous pollutants. The 95% uncertainty intervals were −68.6% to +69.3% and −69.8% to +68.6% for cement PM_{10} and $PM_{2.5}$, as well as −70.7% to +70.1% and −73.2% to +72.4% for iron and steel PM_{10} and $PM_{2.5}$. By contrast, NOx and SO_2 uncertainties narrowed to approximately ±4% to ±25%. This contrast arises because PM estimates rely heavily on process-specific EFs, dust-removal efficiencies, and particle size partitioning assumptions-parameters carrying large sectoral

https://doi.org/10.5194/essd-2026-570
Preprint. Discussion started: 27 July 2026

variability (Liu et al., 2021). NOx and SO_2 emissions are far better constrained by stable combustion chemistry, fuel sulfur/nitrogen contents, and stack-level monitoring or control information, as shown by recent CEMS-based industrial emission datasets (Tang et al., 2023).

3.4.3 Spatial emission comparison against activity-adjusted MEIC

Figures 8 and 9 visualize spatial emission intensity distributions of $PM_{2.5}$, BC, NOx, and SO_2 estimated in this study and activity-adjusted MEIC inventory for cement and iron and steel sectors, respectively. Corresponding comparisons for PM_{10} and CO are provided in Supplementary Figures S1 and S2. Broadly consistent high-emission hotspot locations were identified across both inventories, concentrated within the North China Plain, Yangtze River Delta, Sichuan Basin, Central China, and parts of Northeast China. However, grid-level emission magnitudes diverged sharply especially for particulate pollutants, indicating that matching regional hotspot locations do not guarantee consistent grid-scale emission intensities.

For the cement sector, this study generally estimated lower $PM_{2.5}$, PM_{10}, and BC emissions than the activity-adjusted MEIC inventory across most cement-producing regions, especially in eastern and central China. NOx and SO_2 exhibited mixed positive and negative spatial biases, indicating highly heterogeneous regional discrepancies for them. For iron and steel sector, $PM_{2.5}$, PM_{10}, BC and CO emissions were uniformly lower in our dataset across most major steel-producing regions, particularly in northern and eastern China, while NOx and SO_2 spatial differences displayed strong regional variability.

Pollutant-specific parameter differences partly explain these spatial mismatches. Previous cement inventory research confirms that PM emissions are highly sensitive to process-specific EFs, PM size partitioning ratios, and dust removal efficiencies (Liu et al., 2021). Unit-based studies on iron and steel emissions also highlights the importance of sub-process parameters for accurate estimation (Wang et al., 2019; Wu et al., 2024b).

Differences in spatial allocation methodology provides another important explanation for grid-level discrepancies. This study allocated total industrial emissions to exact grid cells via Point-Of-Interest (POI) factory location datasets, assigning each cement and steel plant to its precise geographic point before gridding. In contrast, activity-adjusted MEIC inventory retained its original

https://doi.org/10.5194/essd-2026-570
Preprint. Discussion started: 27 July 2026

proxy-based spatial distribution scheme, then the adjustment changed the activity magnitude without relocating individual point sources according to updated POI geolocations. Even with identical regional aggregate activity volumes, this mismatch shifts emission allocation across grid cells. This spatial bias disproportionately impacts industrial point sources, as factory coordinates often deviate drastically from population or other proxy-based spatial weightings. Zheng et al. (2021) demonstrated that integrating industrial point sources into MEIC substantially increased point-source contributions of SO_2, NOx, $PM_{2.5}$, and PM_{10} and improved local hotspot representation. Recent INTAC inventory results similarly confirmed that replacing proxy-based allocation with facility geolocations can reduce fine-scale spatial misallocation of industrial emissions in MEIC (Wu et al., 2024a). POI geolocation frameworks have also been proposed to refine spatial distribution of industrial energy consumption and associated pollutant emissions (Li et al., 2019). Consistent regional hotspot patterns between the two inventories reflect matching regional industrial activity, while residual grid-level intensity gaps originate from updated measurement-derived emission parameters and divergent spatial allocation input datasets and methodologies.

https://doi.org/10.5194/essd-2026-570
Preprint. Discussion started: 27 July 2026

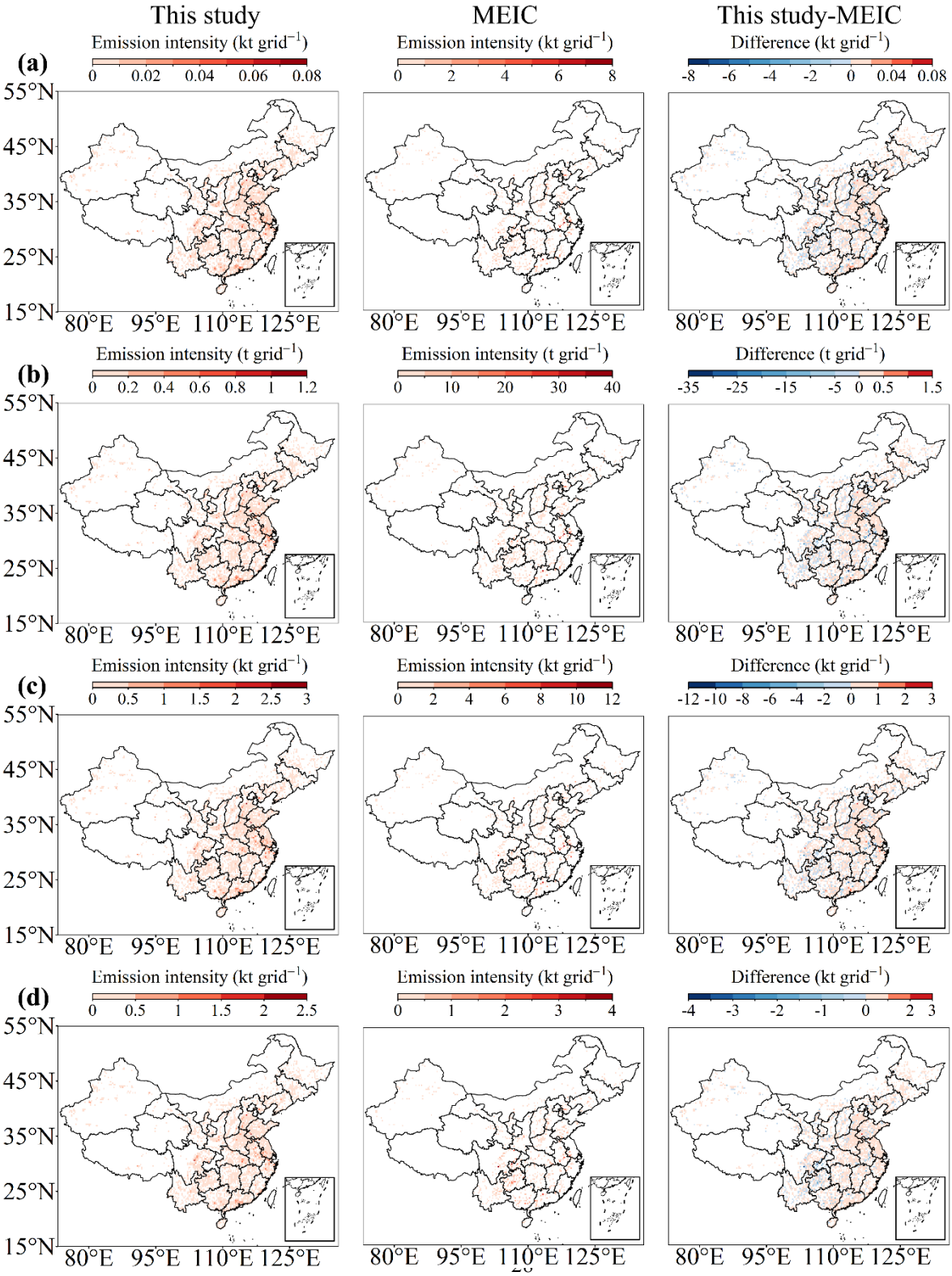

https://doi.org/10.5194/essd-2026-570
Preprint. Discussion started: 27 July 2026

552 Figure 8. Spatial comparison of air pollutant emissions from the cement sector between this study
553 and the activity-adjusted MEIC 2024 inventory. Rows correspond to (a) $PM_{2.5}$, (b) BC, (c) NOx,
554 and (d) SO_2. The columns show the spatial distribution obtained in this study, the activity-adjusted
555 MEIC inventory, and the differences, respectively. Emissions are presented as gridded emission
556 intensities, with units shown in the colour bars. The difference panels represent this study minus the
557 activity-adjusted MEIC inventory.

558

https://doi.org/10.5194/essd-2026-570
Preprint. Discussion started: 27 July 2026

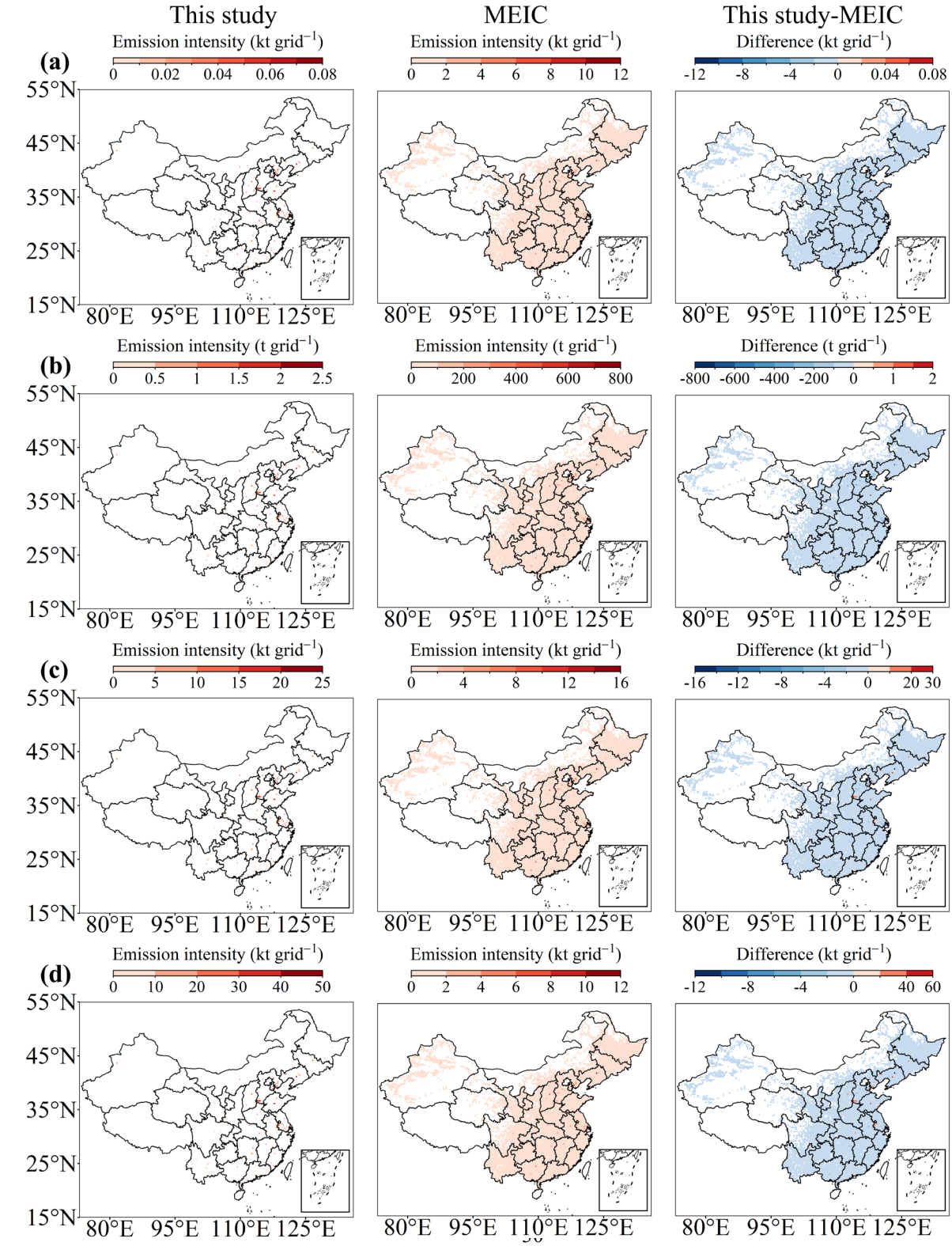

https://doi.org/10.5194/essd-2026-570
Preprint. Discussion started: 27 July 2026

Figure 9. Spatial comparison of air pollutant emissions from the iron and steel sector between this study and the activity-adjusted MEIC 2024 inventory. Rows correspond to (a) $PM_{2.5}$, (b) BC, (c) NOx, and (d) SO_2. The columns show the spatial distribution obtained in this study, the activity-adjusted MEIC 2024 inventory, and their differences, respectively. Emissions are presented as gridded emission intensities, with units shown in the colour bar. The difference panels represent this study minus the activity-adjusted MEIC inventory.

3.5 Limitations of this study

Several key limitations and inherent uncertainties associated with this study should be acknowledged. (1) PM mass concentrations were derived from optical particle measurements, which depend on assumptions regarding particle density, morphology, hygroscopicity, and refractive index. These assumptions introduce systematic uncertainties into measured PM concentrations and corresponding EFs (Hagan and Kroll, 2020). (2) Each industrial facility was monitored for only 3 consecutive days, so the measured EFs may not fully represent annual operating conditions. Seasonal changes in production load and periodic startup/shutdown alter stack pollutant emission concentrations and control equipment performance (Tang et al., 2023). (3) Field measurements covered selected post-control stack outlets rather than full emission boundaries of each sector. Unorganized fugitive emissions and other process outlets, especially for PM from raw material handling, storage, and transportation, were not fully captured here (Liu et al., 2021). (4) The POI data used for spatial allocation reflected facility information available at the time of collection rather than a historical snapshot for 2024. This temporal mismatch may introduce uncertainty into grid-level emissions because industrial point-source locations can strongly affect high-resolution gridded emission distribution (Li et al., 2019; Wu et al., 2024a; Zheng et al., 2021). Future research should extend continuous field measurements across multiple seasons, additional enterprises, diverse process outlets, and fugitive emissions, together with improved year-specific facility status and activity datasets to reduce the above uncertainties.

https://doi.org/10.5194/essd-2026-570
Preprint. Discussion started: 27 July 2026

Open Access Earth System Science Data Discussions

4. Conclusions

This study provides field-measured emission factors and hourly temporal allocation factors for seven stack air pollutants of five industrial sectors in China. Industrial EFs exhibit extreme facility- and pollutant-specific heterogeneity, with our measured values deviating from literature and official guideline values by 1–4 orders of magnitude. BC EFs ranged from 3.2×10^{-6} to 4.7×10^{-2} g kg^{-1} product across the five sectors, yet current inventory guidelines assign zero BC EFs to most corresponding industrial categories. Measured BC/$PM_{2.5}$ mass ratios for cement and iron and steel reached only 0.0136 and 0.0104, respectively, suggesting that literature-derived ratios substantially overestimate BC emissions from modern well-controlled industrial stacks.

$PM_{2.5}$ emissions estimated in this study with our updated EFs were 29.6 and 255 times lower than activity-adjusted MEIC for cement and iron and steel, respectively, whereas the discrepancies for gaseous pollutants were far smaller and displayed pollutant-dependent biases. These results confirm that industrial PM emissions are not solely determined by total production activity, but strongly modulated by field-measured EFs, particulate control efficiency assumptions, covered source categories, and spatial allocation methods. Our PM emission estimates strictly represent organized post-control stack emissions. Comprehensive sector-wide PM emissions still require better integration of fugitive and other non-stack sources. Measured hourly allocation factors displayed clear diurnal variability. $PM_{2.5}$ hourly weights ranged from 0.016 to 0.055, corresponding to deviations of −61.6% to +32.0% relative to the uniform static allocation weight of 1/24. This demonstrates that constant temporal allocation assumptions fail to capture short-term emission spikes, particularly evening enhancements in particulate emissions.

The field-measured EFs and pollutant-resolved hourly diurnal profiles developed here provide robust observational constraints to improve high-temporal-resolution industrial emission inventories, and evaluate industrial contributions via receptor models or air quality simulations, and targeted short-term industrial pollution control policy evaluation.

https://doi.org/10.5194/essd-2026-570
Preprint. Discussion started: 27 July 2026

Data availability

The dataset described in this manuscript (Wang et al., 2026) is available for anonymous peer review through the temporary Zenodo review link:
https://zenodo.org/records/21396152?preview=1&token=eyJhbGciOiJIUzUxMiJ9.eyJpZCI6ImRkZTBmN2Q5LTdiMmEtNDUzZC1hMDgwLWJkZDc3MzgwMGFmNCIsImRhdGEiOnt9LCJyYW5kb20iOiJhZjM4YmMwMzg5NzJlYjJjN2ZjYjAzYjNjNjgwODhkNCJ9.oDB98C00t1i0J3wsd9QP870sLLSC09qXQQOdaFwmV0r910apq2Lx7rr6MrxehSfVGYKFb11JQdBJHDcmHWeIzQ.
The dataset will be made publicly available on Zenodo under the CC BY 4.0 licence, with the reserved DOI: https://doi.org/10.5281/zenodo.21396152, before final publication of the article.

Author contribution

TW conducted the investigation, curated and analyzed the data, prepared the figures, and wrote the manuscript. SK conceptualized and supervised the study, acquired funding, and reviewed and edited the manuscript. XQ, YZ, YF, YY, JW, WL, and FD contributed to the investigation and data collection. All authors reviewed and approved the final manuscript.

Competing interests

The authors declare that they have no conflict of interest.

Acknowledgements

This research has been supported by the National Key Research and Development Program of China (grant nos. 2024YFC3713600 and 2023YFC3709802) and the National Natural Science Foundation of China (grant no. 42575130).

https://doi.org/10.5194/essd-2026-570
Preprint. Discussion started: 27 July 2026

References

Bo, X., Li, Z., Qu, J., Cai, B., Zhou, B., Sun, L., Cui, W., Zhao, X., Tian, J., and Kan, H.: The spatial-temporal pattern of sintered flue gas emissions in iron and steel enterprises of China, J. Clean. Prod., 266, 121667, https://doi.org/10.1016/j.jclepro.2020.121667, 2020.

Bo, X., Jia, M., Xue, X., Tang, L., Mi, Z., Wang, S., Cui, W., Chang, X., Ruan, J., Dong, G., Zhou, B., and Davis, S. J.: Effect of strengthened standards on Chinese ironmaking and steelmaking emissions, Nat. Sustain., 4, 811–820, https://doi.org/10.1038/s41893-021-00736-0, 2021.

Bond, T. C., Doherty, S. J., Fahey, D. W., Forster, P. M., Berntsen, T., DeAngelo, B. J., Flanner, M. G., Ghan, S., Kärcher, B., Koch, D., Kinne, S., Kondo, Y., Quinn, P. K., Sarofim, M. C., Schultz, M. G., Schulz, M., Venkataraman, C., Zhang, H., Zhang, S., Bellouin, N., Guttikunda, S. K., Hopke, P. K., Jacobson, M. Z., Kaiser, J. W., Klimont, Z., Lohmann, U., Schwarz, J. P., Shindell, D., Storelvmo, T., Warren, S. G., and Zender, C. S.: Bounding the role of black carbon in the climate system: A scientific assessment, J. Geophys. Res.-Atmos., 118, 5380–5552, https://doi.org/10.1002/jgrd.50171, 2013.

Brooks, N., Biswas, D., Maithel, S., Miller, G., Mahajan, A., Uddin, M. R., Ahmed, S., Mahzab, M., Rahman, M., and Luby, S. P.: Reducing emissions and air pollution from informal brick kilns: Evidence from Bangladesh, Science, 388, eadr7394, https://doi.org/10.1126/science.adr7394, 2025.

Cai, J., Jiang, H., Chen, Y., Liu, Z., Han, Y., Shen, H., Song, J., Li, J., Zhang, Y., Wang, R., Chen, J., and Zhang, G.: Char dominates black carbon aerosol emission and its historic reduction in China, Nat. Commun., 14, 6444, https://doi.org/10.1038/s41467-023-42192-8, 2023.

Chen, S., Li, J., You, Q., Wang, Z., Shan, W., Bo, X., and Zhu, R.: Improving the air quality management: The air pollutant and carbon emission and air quality model for air pollutant and carbon emission reduction in the iron and steel industries of Tangshan, Hebei Province, China, Atmosphere, 14, 1747, https://doi.org/10.3390/atmos14121747, 2023.

Crippa, M., Guizzardi, D., Muntean, M., Schaaf, E., Dentener, F., Van Aardenne, J. A., Monni, S., Doering, U., Olivier, J. G. J., Pagliari, V., and Janssens-Maenhout, G.: Gridded emissions of

https://doi.org/10.5194/essd-2026-570
Preprint. Discussion started: 27 July 2026

air pollutants for the period 1970–2012 within EDGAR v4.3.2, Earth Syst. Sci. Data, 10, 1987–2013, https://doi.org/10.5194/essd-10-1987-2018, 2018.

Crippa, M., Solazzo, E., Huang, G., Guizzardi, D., Koffi, E., Muntean, M., Schieberle, C., Friedrich, R., and Janssens-Maenhout, G.: High resolution temporal profiles in the Emissions Database for Global Atmospheric Research, Sci. Data, 7, 121, https://doi.org/10.1038/s41597-020-0462-2, 2020.

Drinovec, L., Močnik, G., Zotter, P., Prévôt, A. S. H., Ruckstuhl, C., Coz, E., Rupakheti, M., Sciare, J., Müller, T., Wiedensohler, A., and Hansen, A. D. A.: The "dual-spot" Aethalometer: an improved measurement of aerosol black carbon with real-time loading compensation, Atmos. Meas. Tech., 8, 1965–1979, https://doi.org/10.5194/amt-8-1965-2015, 2015.

Du, Q., Zhao, C., Zhang, M., Dong, X., Chen, Y., Liu, Z., Hu, Z., Zhang, Q., Li, Y., Yuan, R., and Miao, S.: Modeling diurnal variation of surface $PM_{2.5}$ concentrations over East China with WRF-Chem: impacts from boundary-layer mixing and anthropogenic emission, Atmos. Chem. Phys., 20, 2839–2863, https://doi.org/10.5194/acp-20-2839-2020, 2020.

European Environment Agency: EMEP/EEA air pollutant emission inventory guidebook 2023: Cement production, European Environment Agency, 2023.

Geng, G., Liu, Y., Liu, Y., Liu, S., Cheng, J., Yan, L., Wu, N., Hu, H., Tong, D., Zheng, B., Yin, Z., He, K., and Zhang, Q.: Efficacy of China's clean air actions to tackle $PM_{2.5}$ pollution between 2013 and 2020, Nat. Geosci., 17, 987–994, https://doi.org/10.1038/s41561-024-01540-z, 2024.

Govardhan, G., Satheesh, S. K., Moorthy, K. K., and Nanjundiah, R.: Simulations of black carbon over the Indian region: improvements and implications of diurnality in emissions, Atmos. Chem. Phys., 19, 8229–8241, https://doi.org/10.5194/acp-19-8229-2019, 2019.

Gu, X., Li, B., Sun, C., Liao, H., Zhao, Y., and Yang, Y.: An improved hourly-resolved NOx emission inventory for power plants based on continuous emission monitoring system (CEMS) database: A case in Jiangsu, China, J. Clean. Prod., 369, 133176, https://doi.org/10.1016/j.jclepro.2022.133176, 2022.

Guevara, M., Jorba, O., Tena, C., Denier Van Der Gon, H., Kuenen, J., Elguindi, N., Darras, S., Granier, C., and Pérez García-Pando, C.: Copernicus Atmosphere Monitoring Service

https://doi.org/10.5194/essd-2026-570
Preprint. Discussion started: 27 July 2026

TEMPOral profiles (CAMS-TEMPO): global and European emission temporal profile maps for atmospheric chemistry modelling, Earth Syst. Sci. Data, 13, 367–404, https://doi.org/10.5194/essd-13-367-2021, 2021.

Guevara, M., Colette, A., Guion, A., Petiot, V., Adani, M., Arteta, J., Benedictow, A., Bergström, R., Bolignano, A., Camps, P., Carvalho, A., Christensen, J. H., and Couvidat, F.: Technical note: sensitivity of the CAMS regional air quality modelling system to anthropogenic emission temporal variability, Atmos. Chem. Phys., 25, 13245–13278, https://doi.org/10.5194/acp-25-13245-2025, 2025.

Guo, Z., Hao, Y., Tian, H., Bai, X., Wu, B., Liu, S., Luo, L., Liu, W., Zhao, S., Lin, S., Lv, Y., Yang, J., and Xiao, Y.: Field measurements on emission characteristics, chemical profiles, and emission factors of size-segregated PM from cement plants in China, Sci. Total Environ., 818, 151822, https://doi.org/10.1016/j.scitotenv.2021.151822, 2022.

Hagan, D. H. and Kroll, J. H.: Assessing the accuracy of low-cost optical particle sensors using a physics-based approach, Atmos. Meas. Tech., 13, 6343–6355, https://doi.org/10.5194/amt-13-6343-2020, 2020.

Hu, Y., Li, Z., Wang, L., Zhu, H., Chen, L., Guo, X., An, C., Jiang, Y., and Liu, A.: Emission Factors of NOx, SO_2, PM and VOCs in Pharmaceuticals, Brick and Food Industries in Shanxi, China, Aerosol Air Qual. Res., 19, 1785–1797, https://doi.org/10.4209/aaqr.2019.06.0304, 2019.

Hua, S., Tian, H., Wang, K., Zhu, C., Gao, J., Ma, Y., Xue, Y., Wang, Y., Duan, S., and Zhou, J.: Atmospheric emission inventory of hazardous air pollutants from China's cement plants: Temporal trends, spatial variation characteristics and scenario projections, Atmos. Environ., 128, 1–9, https://doi.org/10.1016/j.atmosenv.2015.12.056, 2016.

Huang, Y.-M., Huang, S.-H., Lin, C.-W., Yang, H.-H., and Chen, C.-C.: Evaluation of Bias in the Measurement of Condensable Particulate Matter with Method 202, Aerosol Air Qual. Res., 21, 200149, https://doi.org/10.4209/aaqr.2020.04.0149, 2021.

Jia, J., Cheng, S., Yao, S., Xu, T., Zhang, T., Ma, Y., Wang, H., and Duan, W.: Emission characteristics and chemical components of size-segregated particulate matter in iron and steel

https://doi.org/10.5194/essd-2026-570
Preprint. Discussion started: 27 July 2026

industry, Atmos. Environ., 182, 115–127, https://doi.org/10.1016/j.atmosenv.2018.03.051, 2018.

Karplus, V. J., Zhang, S., and Almond, D.: Quantifying coal power plant responses to tighter SO_2 emissions standards in China, Proc. Natl. Acad. Sci. U.S.A., 115, 7004–7009, https://doi.org/10.1073/pnas.1800605115, 2018.

Klimont, Z., Kupiainen, K., Heyes, C., Purohit, P., Cofala, J., Rafaj, P., Borken-Kleefeld, J., and Schöpp, W.: Global anthropogenic emissions of particulate matter including black carbon, Atmos. Chem. Phys., 17, 8681–8723, https://doi.org/10.5194/acp-17-8681-2017, 2017.

Kong, L., Tang, X., Wang, Z., Zhu, J., Li, J., Wu, H., Wu, Q., Chen, H., Zhu, L., Wang, W., Liu, B., Wang, Q., Chen, D., Pan, Y., Li, J., Wu, L., and Carmichael, G. R.: Changes in air pollutant emissions in China during two clean-air action periods derived from the newly developed Inversed Emission Inventory for Chinese Air Quality (CAQIEI), Earth Syst. Sci. Data, 16, 4351–4387, https://doi.org/10.5194/essd-16-4351-2024, 2024.

Kong, S., Ji, Y., Li, Z., Lu, B., and Bai, Z.: Emission and profile characteristic of polycyclic aromatic hydrocarbons in $PM_{2.5}$ and PM_{10} from stationary sources based on dilution sampling, Atmos. Environ., 77, 155–165, https://doi.org/10.1016/j.atmosenv.2013.04.073, 2013.

Kurokawa, J., Ohara, T., Morikawa, T., Hanayama, S., Janssens-Maenhout, G., Fukui, T., Kawashima, K., and Akimoto, H.: Emissions of air pollutants and greenhouse gases over Asian regions during 2000–2008: Regional Emission inventory in ASia (REAS) version 2, Atmos. Chem. Phys., 13, 11019–11058, https://doi.org/10.5194/acp-13-11019-2013, 2013.

Lei, Y., Zhang, Q., Nielsen, C., and He, K.: An inventory of primary air pollutants and CO_2 emissions from cement production in China, 1990–2020, Atmos. Environ., 45, 147–154, https://doi.org/10.1016/j.atmosenv.2010.09.034, 2011.

Li, B., Wang, J., Wu, S., Jia, Z., Li, Y., Wang, T., and Zhou, S.: New Method for Improving Spatial Allocation Accuracy of Industrial Energy Consumption and Implications for Polycyclic Aromatic Hydrocarbon Emissions in China, Environ. Sci. Technol., 53, 4326–4334, https://doi.org/10.1021/acs.est.8b06915, 2019.

https://doi.org/10.5194/essd-2026-570
Preprint. Discussion started: 27 July 2026

Li, S., Wang, S., Wu, Q., Zhang, Y., Ouyang, D., Zheng, H., Han, L., Qiu, X., Wen, Y., Liu, M., Jiang, Y., Yin, D., Liu, K., Zhao, B., Zhang, S., Wu, Y., and Hao, J.: Emission trends of air pollutants and CO_2 in China from 2005 to 2021, Earth Syst. Sci. Data, 15, 2279–2294, https://doi.org/10.5194/essd-15-2279-2023, 2023.

Liu, F., Zhang, Q., Tong, D., Zheng, B., Li, M., Huo, H., and He, K. B.: High-resolution inventory of technologies, activities, and emissions of coal-fired power plants in China from 1990 to 2010, Atmos. Chem. Phys., 15, 13299–13317, https://doi.org/10.5194/acp-15-13299-2015, 2015.

Liu, F., Yu, D., Han, J., Wu, J., Yu, X., and Gong, X.: Effects of ultra-low emission air pollution control devices on the evolution of PM and its associated water-soluble ions in a 1000 MW coal-fired power plant, Fuel, 343, 127931, https://doi.org/10.1016/j.fuel.2023.127931, 2023.

Liu, H., Wu, B., Liu, S., Shao, P., Liu, X., Zhu, C., Wang, Y., Wu, Y., Xue, Y., Gao, J., Hao, Y., and Tian, H.: A regional high-resolution emission inventory of primary air pollutants in 2012 for Beijing and the surrounding five provinces of North China, Atmos. Environ., 181, 20–33, https://doi.org/10.1016/j.atmosenv.2018.03.013, 2018.

Liu, H., Yang, F., Du, Y., Ruan, R., Tan, H., Xiao, J., and Zhang, S.: Field measurements on particle size distributions and emission characteristics of PM_{10} in a cement plant of China, Atmos. Pollut. Res., 10, 1464–1472, https://doi.org/10.1016/j.apr.2019.04.003, 2019.

Liu, J., Tong, D., Zheng, Y., Cheng, J., Qin, X., Shi, Q., Yan, L., Lei, Y., and Zhang, Q.: Carbon and air pollutant emissions from China's cement industry 1990–2015: trends, evolution of technologies, and drivers, Atmos. Chem. Phys., 21, 1627–1647, https://doi.org/10.5194/acp-21-1627-2021, 2021.

Liu, J., Wang, S., Yi, H., Tang, X., Li, Z., Yu, Q., Zhao, S., Gao, F., Zhou, Y., and Wang, Y.: Air pollutant emission and reduction potentials from the sintering process of the iron and steel industry in China in 2017, Environ. Pollut., 307, 119512, https://doi.org/10.1016/j.envpol.2022.119512, 2022.

https://doi.org/10.5194/essd-2026-570
Preprint. Discussion started: 27 July 2026

771 Liu, X., Yang, L., Du, J., Zhang, H., Hu, J., Chen, A., and Lv, W.: Carbon and air pollutant
772 emissions forecast of China's cement industry from 2021 to 2035, Resour. Conserv. Recycl.,
773 204, 107498, https://doi.org/10.1016/j.resconrec.2024.107498, 2024.
774 McDuffie, E. E., Smith, S. J., O'Rourke, P., Tibrewal, K., Venkataraman, C., Marais, E. A., Zheng,
775 B., Crippa, M., Brauer, M., and Martin, R. V.: A global anthropogenic emission inventory of
776 atmospheric pollutants from sector- and fuel-specific sources (1970–2017): an application of
777 the Community Emissions Data System (CEDS), Earth Syst. Sci. Data, 12, 3413–3442,
778 https://doi.org/10.5194/essd-12-3413-2020, 2020.
779 Ministry of Ecology and Environment of China: Technical guideline on city-level air pollutant
780 emission inventory development, Ministry of Ecology and Environment of the People's
781 Republic of China, Beijing, China, 2024.
782 Ministry of Ecology and Environment of China, National Development and Reform Commission,
783 Ministry of Industry and Information Technology, Ministry of Finance, and Ministry of
784 Transport: Opinions on promoting the implementation of ultra-low emissions in the iron and
785 steel industry, Ministry of Ecology and Environment of China, Beijing, China, 2019.
786 Ministry of Ecology and Environment of China, National Development and Reform Commission,
787 Ministry of Industry and Information Technology, Ministry of Finance, and Ministry of
788 Transport: Opinions on promoting the implementation of ultra-low emissions in the cement
789 industry, Ministry of Ecology and Environment of China, Beijing, China, 2024.
790 Ohara, T., Akimoto, H., Kurokawa, J., Horii, N., Yamaji, K., Yan, X., and Hayasaka, T.: An Asian
791 emission inventory of anthropogenic emission sources for the period 1980–2020, Atmos.
792 Chem. Phys., 7, 4419–4444, https://doi.org/10.5194/acp-7-4419-2007, 2007.
793 Olivier, J. G. J., Bouwman, A. F., van der Maas, C. W. M., and M., B., J. J.: Emission database for
794 global atmospheric research (EDGAR), Environ. Monit. Assess., 31, 93–106,
795 https://doi.org/10.1007/BF00547184, 1994.
796 Petzold, A., Ogren, J. A., Fiebig, M., Laj, P., Li, S.-M., Baltensperger, U., Holzer-Popp, T., Kinne,
797 S., Pappalardo, G., Sugimoto, N., Wehrli, C., Wiedensohler, A., and Zhang, X.-Y.:

https://doi.org/10.5194/essd-2026-570
Preprint. Discussion started: 27 July 2026

Recommendations for reporting “black carbon” measurements, Atmos. Chem. Phys., 13, 8365–8379, https://doi.org/10.5194/acp-13-8365-2013, 2013.

Pham, T. B. T., Manomaiphiboon, K., and Vongmahadlek, C.: Development of an inventory and temporal allocation profiles of emissions from power plants and industrial facilities in Thailand, Sci. Total Environ., 397, 103–118, https://doi.org/10.1016/j.scitotenv.2008.01.066, 2008.

Pileci, R. E., Modini, R. L., Bertò, M., Yuan, J., Corbin, J. C., Marinoni, A., Henzing, B., Moerman, M. M., Putaud, J. P., Spindler, G., Wehner, B., Müller, T., Tuch, T., Trentini, A., Zanatta, M., Baltensperger, U., and Gysel-Beer, M.: Comparison of co-located refractory black carbon (rBC) and elemental carbon (EC) mass concentration measurements during field campaigns at several European sites, Atmos. Meas. Tech., 14, 1379–1403, https://doi.org/10.5194/amt-14-1379-2021, 2021.

Qin, X., Kong, S., Wu, J., Yan, Q., Yan, Y., Zheng, S., Cheng, Y., and Qi, S.: Hourly emission of submicron particulate matter from residential coal combustion and its potential health impacts in China, J. Geophys. Res.-Atmos., 131, e2026JD046630, https://doi.org/10.1029/2026JD046630, 2026.

Saikawa, E., Kim, H., Zhong, M., Avramov, A., Zhao, Y., Janssens-Maenhout, G., Kurokawa, J., Klimont, Z., Wagner, F., Naik, V., Horowitz, L. W., and Zhang, Q.: Comparison of emissions inventories of anthropogenic air pollutants and greenhouse gases in China, Atmos. Chem. Phys., 17, 6393–6421, https://doi.org/10.5194/acp-17-6393-2017, 2017.

Schiferl, L. D., Cao, C., Dalton, B., Hallward-Driemeier, A., Toledo-Crow, R., and Commane, R.: Multi-year observations of variable incomplete combustion in the New York megacity, Atmos. Chem. Phys., 24, 10129–10142, https://doi.org/10.5194/acp-24-10129-2024, 2024.

Solazzo, E., Crippa, M., Guizzardi, D., Muntean, M., Choulga, M., and Janssens-Maenhout, G.: Uncertainties in the Emissions Database for Global Atmospheric Research (EDGAR) emission inventory of greenhouse gases, Atmos. Chem. Phys., 21, 5655–5683, https://doi.org/10.5194/acp-21-5655-2021, 2021.

Sowden, M., Cairncross, E., Wilson, G., Zunckel, M., Kirillova, E., Reddy, V., and Hietkamp, S.: Developing a spatially and temporally resolved emission inventory for photochemical

https://doi.org/10.5194/essd-2026-570
Preprint. Discussion started: 27 July 2026

modeling in the City of Cape Town and assessing its uncertainty, Atmos. Environ., 42, 7155–7164, https://doi.org/10.1016/j.atmosenv.2008.05.048, 2008.

Sun, C., Li, B., Chen, L., Gao, Y., Jin, J., Gu, X., Yang, Y., Lou, Y., Zhao, Y., and Liao, H.: An improved hourly-resolved atmospheric NOx emission inventory of industrial sources based on Continuous Emission Monitoring System data: Case of Jiangsu Province, China, J. Clean. Prod., 419, 138192, https://doi.org/10.1016/j.jclepro.2023.138192, 2023.

Tang, L., Xue, X., Jia, M., Jing, H., Wang, T., Zhen, R., Huang, M., Tian, J., Guo, J., Li, L., Bo, X., and Wang, S.: Iron and steel industry emissions and contribution to the air quality in China, Atmos. Environ., 237, 117668, https://doi.org/10.1016/j.atmosenv.2020.117668, 2020.

Tang, L., Jia, M., Yang, J., Li, L., Bo, X., and Mi, Z.: Chinese industrial air pollution emissions based on the continuous emission monitoring systems network, Sci. Data, 10, 153, https://doi.org/10.1038/s41597-023-02054-w, 2023.

Tang, L., Yu, Q., Qu, J., Wan, R., Jia, M., Qian, S., Lv, S., Li, J., and Qi, S.: Synergistic air pollution and CO_2 emission reduction in China's iron and steel industry based on real-time monitoring data, Environ. Pollut., 385, 127053, https://doi.org/10.1016/j.envpol.2025.127053, 2025.

U.S. Environmental Protection Agency: 2016v2 emissions modeling platform: temporal allocation profiles, U.S. Environmental Protection Agency, 2021.

Wang, T., Kong, S., Qin, X., Zhou, Y., Feng, Y., Yan, Y., Wu, J., Liu, W., and Ding, F.: Field-tested emission factors and temporal allocation factors for air pollutants emitted from industrial sources in China, https://doi.org/10.5281/zenodo.21396152, 2026.

Wang, X., Lei, Y., Yan, L., Liu, T., Zhang, Q., and He, K.: A unit-based emission inventory of SO_2, NOx and PM for the Chinese iron and steel industry from 2010 to 2015, Sci. Total Environ., 676, 18–30, https://doi.org/10.1016/j.scitotenv.2019.04.241, 2019.

Wu, B., Bai, X., Liu, W., Lin, S., Liu, S., Luo, L., Guo, Z., Zhao, S., Lv, Y., Zhu, C., Hao, Y., Liu, Y., Hao, J., Duan, L., and Tian, H.: Non-Negligible Stack Emissions of Noncriteria Air Pollutants from Coal-Fired Power Plants in China: Condensable Particulate Matter and Sulfur

https://doi.org/10.5194/essd-2026-570
Preprint. Discussion started: 27 July 2026

Trioxide, Environ. Sci. Technol., 54, 6540–6550, https://doi.org/10.1021/acs.est.0c00297, 2020.

Wu, N., Geng, G., Xu, R., Liu, S., Liu, X., Shi, Q., Zhou, Y., Zhao, Y., Liu, H., Song, Y., Zheng, J., Zhang, Q., and He, K.: Development of a high-resolution integrated emission inventory of air pollutants for China, Earth Syst. Sci. Data, 16, 2893–2915, https://doi.org/10.5194/essd-16-2893-2024, 2024a.

Wu, W., Tang, Q., Xue, W., Shi, X., Zhao, D., Liu, Z., Liu, X., Jiang, C., Yan, G., and Wang, J.: Quantifying China's iron and steel industry's CO_2 emissions and environmental health burdens: A pathway to sustainable transformation, Environ. Sci. Ecotechnology, 20, 100367, https://doi.org/10.1016/j.ese.2023.100367, 2024b.

Yan, X., Tong, D., Cao, Z., Chen, C., Guo, Y., Xu, R., Qin, X., Fu, Y., Liu, Y., Zheng, D., He, K., and Zhang, Q.: Historical air pollutant emissions and future sustainable pathways of global cement plants, Resour. Conserv. Recycl., 211, 107896, https://doi.org/10.1016/j.resconrec.2024.107896, 2024.

Yi, H., Zhong, T., Liu, J., Yu, Q., Zhao, S., Gao, F., Zhou, Y., Wang, S., and Tang, X.: Emissions of air pollutants from sintering flue gas in the Beijing-Tianjin-Hebei area and proposed reduction measures, J. Clean. Prod., 304, 126958, https://doi.org/10.1016/j.jclepro.2021.126958, 2021.

Yuan, J., Bu, L., Huang, X., Gao, H., and Sa, R.: Particulate Characteristics during a Haze Episode Based on Two Ceilometers with Different Wavelengths, Atmosphere, 7, 20, https://doi.org/10.3390/atmos7020020, 2016.

Zhang, J., Shen, H., Chen, Y., Meng, J., Li, J., He, J., Guo, P., Dai, R., Zhang, Y., Xu, R., Wang, J., Zheng, S., Lei, T., Shen, G., Wang, C., Ye, J., Zhu, L., Sun, H. Z., Fu, T.-M., Yang, X., Guan, D., and Tao, S.: Iron and steel industry emissions: a global analysis of trends and drivers, Environ. Sci. Technol., 57, 16477–16488, https://doi.org/10.1021/acs.est.3c05474, 2023.

Zhang, Q., Zheng, Y., Tong, D., Shao, M., Wang, S., Zhang, Y., Xu, X., Wang, J., He, H., Liu, W., Ding, Y., Lei, Y., Li, J., Wang, Z., Zhang, X., Wang, Y., Cheng, J., Liu, Y., Shi, Q., Yan, L., Geng, G., Hong, C., Li, M., Liu, F., Zheng, B., Cao, J., Ding, A., Gao, J., Fu, Q., Huo, J., Liu,

https://doi.org/10.5194/essd-2026-570
Preprint. Discussion started: 27 July 2026

881 B., Liu, Z., Yang, F., He, K., and Hao, J.: Drivers of improved $PM_{2.5}$ air quality in China from
882 2013 to 2017, Proc. Natl. Acad. Sci. U.S.A., 116, 24463–24469,
883 https://doi.org/10.1073/pnas.1907956116, 2019a.
884 Zhang, T., Wu, C., Li, B., Wang, J., Ravat, R., Chen, X., Wei, J., and Yu, Q.: Linking the SO_2
885 emission of cement plants to the sulfur characteristics of their limestones: A study of 80 NSP
886 cement lines in China, J. Clean. Prod., 220, 200–211,
887 https://doi.org/10.1016/j.jclepro.2019.02.133, 2019b.
888 Zhang, W., Liu, X., Zhang, C., Li, M., Niu, T., Xie, Y., and Wang, H.: Industrial scale testing on
889 the combustion and NO emission characteristics of ammonia cofiring in a 40 MWth coal-fired
890 boiler, Fuel, 359, 130471, https://doi.org/10.1016/j.fuel.2023.130471, 2024.
891 Zhao, Y., Wang, S., Duan, L., Lei, Y., Cao, P., and Hao, J.: Primary air pollutant emissions of coal-
892 fired power plants in China: Current status and future prediction, Atmos. Environ., 42, 8442–
893 8452, https://doi.org/10.1016/j.atmosenv.2008.08.021, 2008.
894 Zhao, Y., Nielsen, C. P., Lei, Y., McElroy, M. B., and Hao, J.: Quantifying the uncertainties of a
895 bottom-up emission inventory of anthropogenic atmospheric pollutants in China, Atmos. Chem.
896 Phys., 11, 2295–2308, https://doi.org/10.5194/acp-11-2295-2011, 2011.
897 Zheng, B., Tong, D., Li, M., Liu, F., Hong, C., Geng, G., Li, H., Li, X., Peng, L., Qi, J., Yan, L.,
898 Zhang, Y., Zhao, H., Zheng, Y., He, K., and Zhang, Q.: Trends in China's anthropogenic
899 emissions since 2010 as the consequence of clean air actions, Atmos. Chem. Phys., 18, 14095–
900 14111, https://doi.org/10.5194/acp-18-14095-2018, 2018.
901 Zheng, B., Cheng, J., Geng, G., Wang, X., Li, M., Shi, Q., Qi, J., Lei, Y., Zhang, Q., and He, K.:
902 Mapping anthropogenic emissions in China at 1 km spatial resolution and its application in air
903 quality modeling, Sci. Bull., 66, 612–620, https://doi.org/10.1016/j.scib.2020.12.008, 2021.
904